

NPS ARCHIVE
1963
LUSK, C.

PHOTOGRAPHIC INVESTIGATION OF
REFLECTED SHOCK PHENOMENA FROM
DECIGRAM EXPLOSIVE CHARGES

CHARLES T. LUSK
and
HUGH L. WEBSTER

PHOTOGRAPHIC INVESTIGATION OF
REFLECTED SHOCK PHENOMENA FROM
DECIGRAM EXPLOSIVE CHARGES

* * * * *

Charles T. Lusk

and

Hugh L. Webster

PHOTOGRAPHIC INVESTIGATION OF
REFLECTED SHOCK PHENOMENA FROM
DECIGRAM EXPLOSIVE CHARGES

by

Charles T. Lusk

Lieutenant, United States Navy

and

Hugh L. Webster

Lieutenant, United States Navy

Submitted in partial fulfillment of
the requirements for the degree of

MASTER OF SCIENCE
IN
CHEMISTRY

United States Naval Postgraduate School
Monterey, California

1 9 6 3

PHOTOGRAPHIC INVESTIGATION OF
REFLECTED SHOCK PHENOMENA FROM
DECIGRAM EXPLOSIVE CHARGES

by

Charles T. Lusk

and

Hugh L. Webster

This work is accepted as fulfilling
the thesis requirements for the degree of

MASTER OF SCIENCE

IN

CHEMISTRY

from the

United States Naval Postgraduate School

ABSTRACT

An investigation of the primary shock front and Mach Y-stem systems was conducted utilizing decigram explosive charges. Distance and arrival time data of the primary shock front was correlated with that of high yield explosions. A good correlation would indicate the feasibility of conducting laboratory scale tests to obtain information on high yield explosions without the expenditure of time and money involved in large scale field tests. The shock front system was also investigated at the time of first formation of the Mach Y-stem. The critical angle of incidence of the primary shock front for the formation of the Y-stem was compared to the theoretical value. Theoretical calculations of the yield of the explosion was also compared to the actual yield.

Basic data were obtained from the explosions by photographing the shadow of the shock front system utilizing a Polaroid camera, a microflash unit and a time delay generator.

Correlation of the overpressure was excellent for small to moderate distances from the point of explosion, as was the yield comparison. The critical angle of incidence comparison indicated a marked difference between experimental and theoretical values.

ACKNOWLEDGEMENT

The assistance and encouragement of Professors G. F. Kinney, C. A. Hering and J. E. Sinclair are gratefully acknowledged.

Further, the technical support and assistance of the Postgraduate School Machine Shop, Photographic Laboratory, and the technicians of the Engineering School Electronics Department were invaluable in the successful completion of this investigation.

TABLE OF CONTENTS

| Section | Title | Page |
|-------------|--------------------------|------|
| 1. | Introduction | 1 |
| 2. | Experimental Setup | 4 |
| 3. | Preparation of Charges | 18 |
| 4. | Experimental Procedure | 24 |
| 5. | Data | 27 |
| 6. | Calculations | 32 |
| 7. | Conclusions | 39 |
| 8. | Bibliography | 44 |
| Appendix I. | Digital Computer Program | 54 |

LIST OF ILLUSTRATIONS

| Figure | Page |
|--|------|
| 1. Photograph of Reflected Shock Front System | 2 |
| 2. Schematic of Reflected Shock Front System | 3 |
| 3. Schematic of Physical Setup | 5 |
| 4. Lamp Unit, Object Camera, Charge, Blast Table, Reflective Screen and Photocells | 7 |
| 5. Firing Circuit | 10 |
| 6. Electronic Components | 10 |
| 7. Charge Die and Press | 19 |
| 8. Low Order Detonation | 27 |
| 9. Diagram for Calculating First Geometric Factor | 28 |
| 10. Diagram for Calculating Second Geometric Factor | 29 |
| 11. Delta Time vs. Radius | 45 |
| 12. Height of Triple Point vs. Time | 46 |
| 13. Distance of Mach Y-Stem from Ground Zero vs. Time | 47 |
| 14. b Ratio vs. Radius | 48 |
| 15. Calculated Yield vs. Radius | 49 |
| 16. Reduced Radius vs. Reduced Time (Brode) | 50 |
| 17. Peak Overpressure vs. Reduced Radius | 51 |
| 18. Reduced Radius vs. Reduced Time | 52 |
| 19. Scaled Radius vs. Scaled Time | 53 |

TABLE OF SYMBOLS AND ABBREVIATIONS

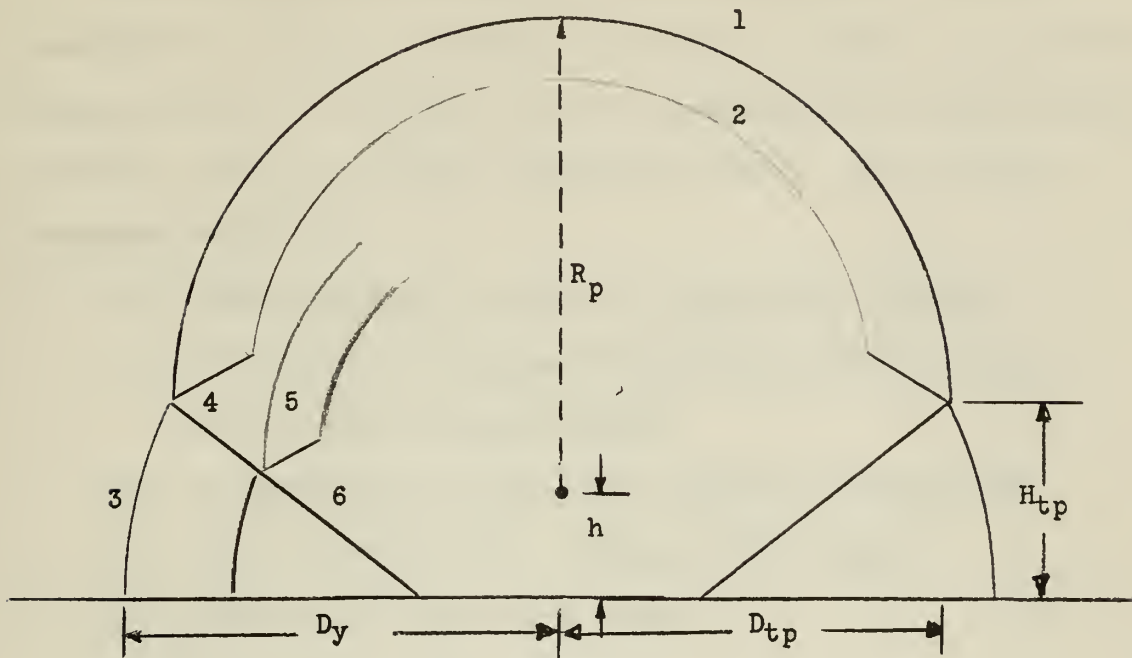
| | | |
|------------|------------------|---|
| a | - cm/sec | - Speed of sound under prevailing ambient conditions |
| b | - ft/millisecond | - Ratio of primary shock front radius to arrival time |
| ΔA | - ergs | - Calculated energy of explosion |
| D_{tp} | - cm | - Horizontal distance from ground zero (point on blast table directly under charge) to triple point |
| D_y | - cm | - Horizontal distance from ground zero to Mach Y-stem |
| f | - dimensionless | - Geometric factor to convert measured parameters from plane of grid screen to plane of charge |
| f_a | - dimensionless | - Transmission factor for the speed of sound |
| f_d | - dimensionless | - Transmission factor for density |
| h | - cm | - Height of charge above blast table |
| H_{tp} | - cm | - Height of triple point above blast table |
| R_p | - cm | - Radius of primary shock front |
| t | - microseconds | - Delay time or arrival time of shock front at an observed radius |
| t_a | - microseconds | - Arrival time of sound at an observed radius |
| Δt | - microseconds | - Difference between t_a and t |
| W | - grams | - Charge weight |
| W_0 | - grams | - Reference charge weight |
| PETN | - | - Pentaerythritol tetranitrate |
| TNT | - | - Trinitrotoluene |
| α | - cm | - Reduced energy parameter |
| λ | - dimensionless | - Reduced radius parameter |
| τ | - dimensionless | - Reduced time parameter |
| ω | - dimensionless | - Yield factor |

1. Introduction

When decigram charges of chemical explosives are detonated, a shock front originates at the point of detonation and expands spherically outward. At a critical angle of incidence of the primary shock front on a reflecting surface, a Mach Y-stem begins to form. This critical angle is dependent upon the Mach number of the incident shock front. The Y-stem is formed when the primary shock front combines with the reflected shock front. As the radius of the shock front continues to increase, the Mach Y-stem grows and travels out from the point of detonation approximately perpendicular to the reflecting surface. This phenomenon can be photographed at different times and distances from the point of detonation and thus, by compiling the data obtained from many successive detonations, a study of the primary shock front and the Mach Y-stem can be achieved. From this study there should result a correlation between small chemical explosions and large point source (nuclear) explosions. A photograph of a well formed Y-stem is shown in Fig. 1. A detailed drawing of the complete shock front system is shown in Fig. 2.



Schematic of Reflected Shock Front System



- | | |
|--------------------------|---------------------------------|
| 1. Primary shock front | 4. Triple point |
| 2. Reflected shock front | 5. Secondary shock front system |
| 3. Mach Y-stem | 6. Slipstream |

Figure 2

2. Experimental Setup

A. The experimental setup had a two fold purpose. First, it contained the necessary electrical circuitry to initiate the explosive charge. Second, it provided a means to photograph the resulting shock front at a preset, accurately measured time delay. The following components were used:

- (1) 1391-B Time Delay Generator - General Radio Company
- (2) 524B Electronic Counter with 526B Time Interval Plug-in Unit - Hewlett Packard Company
- (3) 504 Cathode Ray Oscilloscope - Tektronix Incorporated
- (4) 1530-A Microflash Unit - General Radio Company
- (5) 110B Polaroid Camera with Tripod
- (6) Oscilloscope Camera - Dumont
- (7) Cathetometer
- (8) Two Phototubes - RCA type 868
- (9) 120 Volt Variac - General Radio Company
- (10) Blast Table
- (11) Scotch-brite Reflective Grid Screen
- (12) Two Lab-jacks
- (13) Warning Buzzer
- (14) Test Light

B. To accomplish the above, the apparatus was positioned and connected electrically as shown schematically in Fig. 3.

To better understand the necessity of this particular setup a brief description of the experimental procedure is given.

The basic electronic components were photocell #1, the time delay generator, and the microflash unit. Photocell #2, the CRO and the

Schematic of Physical Setup

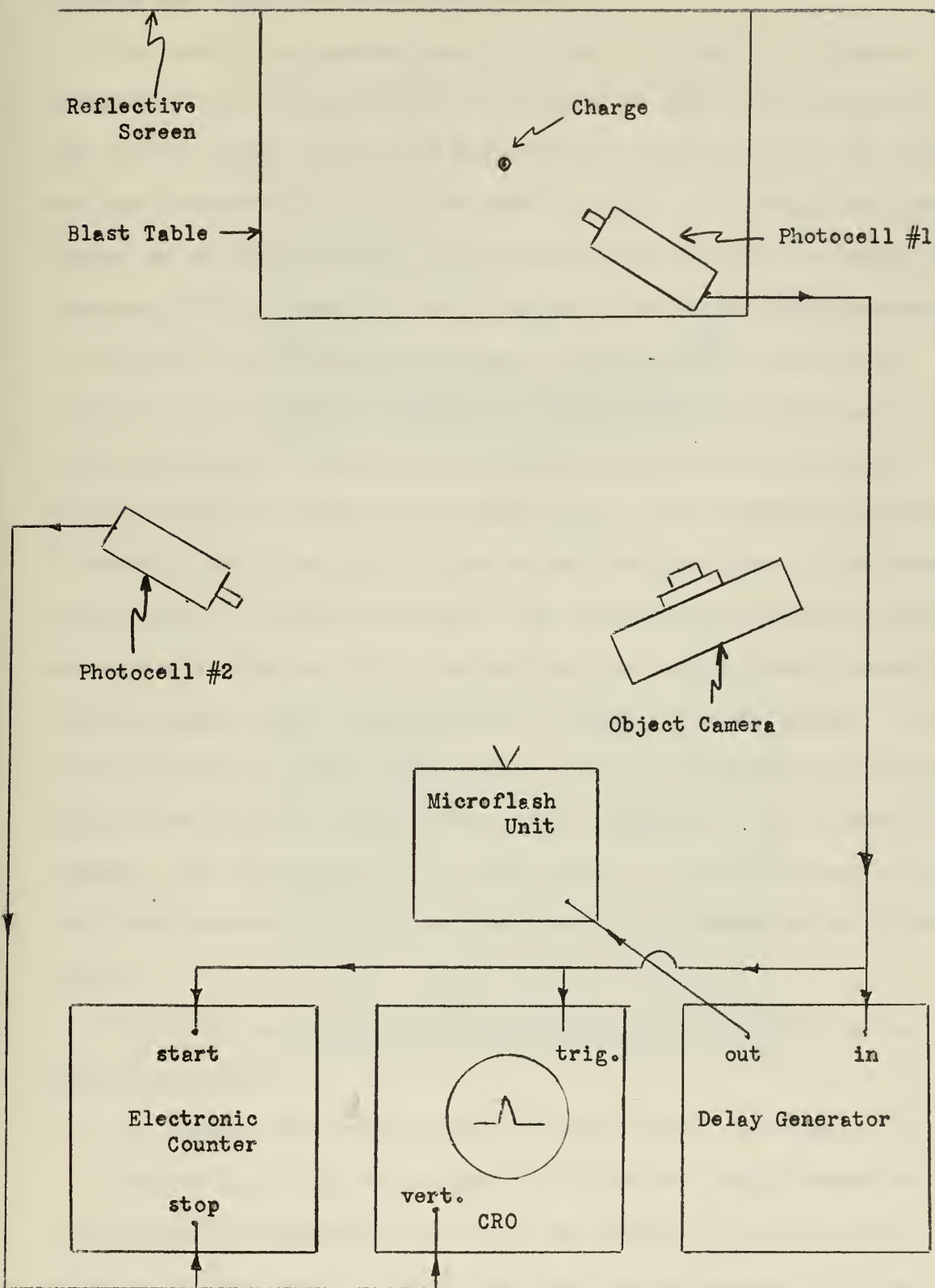


Figure 3

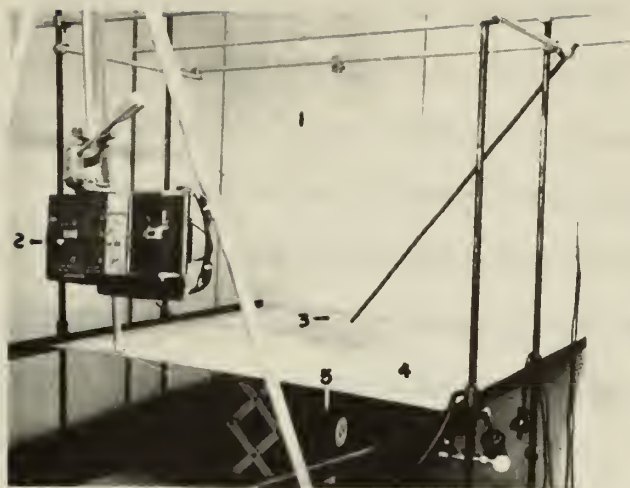
electronic counter were only necessary to determine the true time delay between the explosion and the light flash.

The charge was mounted above the blast table and its alignment checked with the cathetometer. The shutter of both the object camera and the CRO camera were opened manually in a darkened room. The charge was then detonated by closing the switch of the variac which was connected to an AC wall outlet. The blast of the explosion was sensed by photocell #1 which sent the start impulse to the time delay generator, to the start circuit of the electronic counter, and to the trigger circuit of the CRO. The impulse to the time delay generator was delayed a prescribed number of microseconds and then continued to the microflash unit to initiate the light flash. This flash of light cast a shadow of the shock front on the reflective grid screen. The shadow was recorded by the object camera. The light from the microflash unit was sensed by photocell #2. The impulse from this photocell stopped the electronic counter and initiated a vertical blip on the CRO. The true time interval between the explosion and the photographing of the shock front (when the light flashed) was displayed on the electronic counter. The time interval was also recorded on the CRO camera film. The camera shutters were closed after the charge detonation and light flash.

With this operation in mind, the assembly of the apparatus can now be discussed.

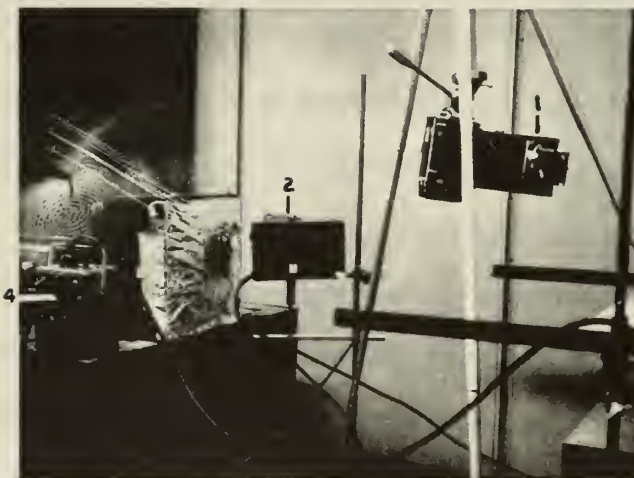
C. Charge, Reflective Screen and Blast Table: See Fig. 4.

The charge of PETN was mounted at the desired height above the blast table by attaching the wires of the charge to the two leads from the firing circuit. These leads were passed through a 1/4 inch



- 1. Grid Screen
- 2. Camera
- 3. Charge
- 4. Blast Table
- 5. Photocell #1

Figure 4a



- 1. Camera
- 2. Photocell #2
- 3. Lamp Unit
- 4. Variac

Figure 4b

copper tube which was at first suspended vertically from a horizontal cross arm. The cross arm was well above the area in which the shock fronts would be photographed. This method of suspension, however, was discarded in favor of a diagonal suspension due to the slight distortion and possible attenuation of the shock front as it passed vertically up the copper tube. Measurement of the primary shock front radius was facilitated by having a pure shock front in the vertical plane directly above the point of explosion. With the diagonal suspension and the flexibility provided by the leads, the charge position could easily be adjusted for exact alignment.

A cathetometer was used to ensure exact alignment of the charge in two dimensions. The desired position of the charge was at a given height directly above a hole centered in the blast table and in line with the microflash unit and the center vertical grid line of the reflective screen. This position was accurately determined before the charge was mounted by the use of a metal centimeter rule placed upright with one edge directly over the center of the blast table hole. The cathetometer was positioned and leveled, but offset horizontally from the center line. This offset was necessary due to interference with the microflash unit and camera which were on or near the center line. The height of the cathetometer was adjusted to the exact desired height of the charge by aligning the crosshairs of the cathetometer with the appropriate centimeter mark on the metal rule. The offset of the cathetometer also required that a bench-mark be accurately inscribed on the grid screen in line with the vertical crosshair of the cathetometer and the vertical edge of the metal rule. Therefore, when mounting the charge it merely had to be positioned so as to coincide with the bench-

mark on the screen and the crosshairs of the cathetometer. The cathetometer was also utilized to check the level of the blast table by moving the metal centimeter rule to the front, to the back and to both sides of the blast table and sighting on the desired centimeter mark of the rule with the cathetometer. The table was level when the desired centimeter mark on the rule coincided with the horizontal crosshair in the cathetometer and the horizontal grid on the reflective screen. The reflective screen was leveled when initially mounted against the wall. The blast table (80 by 85 cm.) was supported on its sides by two "angle iron" beams which were in turn attached by movable clamps to the blast table frame. This frame was given added rigidity by the use of numerous cross and diagonal support rods. Two lab jacks were placed under the center portion of the blast table. These jacks made fine adjustments in height and leveling of the table easier as well as to prevent the blast table from buckling under the force of the explosive blast. This entire apparatus was placed on a solid laboratory table.

To reflect as much light as possible to the object camera, a screen of highly reflective Minnesota-Manufacturing Company Scotch-lite tape was constructed. The tape, in two foot wide strips, was attached to a sheet of 4 x 8 foot plywood. To furnish a grid on the screen for distance measurement purposes, black thread was attached horizontally and vertically at exact intervals of ten centimeters. The completed reflective screen was then mounted and leveled flush against the wall.

D. Firing Circuit. (See Fig. 5)

The variac was connected to a standard wall outlet (115 volt, AC). The variac rheostat was set at 60 volts to ensure adequate

Firing Circuit

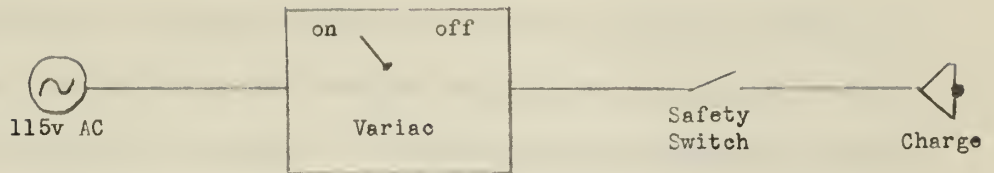
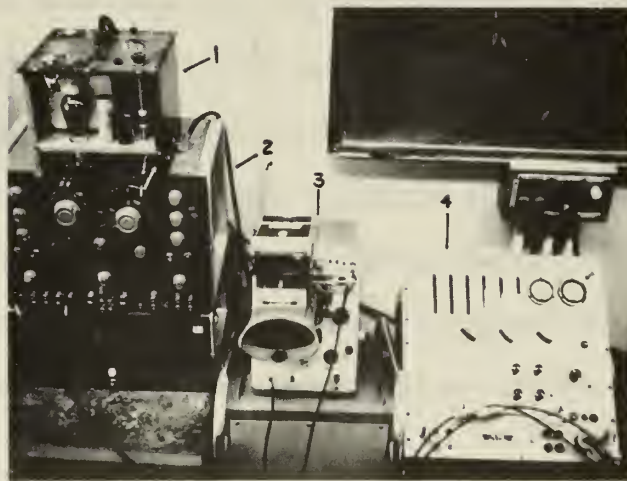


Figure 5



1. Microflash Power Unit
2. Delay Generator
3. CRO
4. Frequency Counter

Figure. 6

current through the charge wire. For safety purposes an extra switch, in addition to that on the variac, was added to the circuit. This switch was closed just prior to opening the camera shutters on each firing and opened immediately after the room lights were turned on after the explosion. The variac switch was used to finally complete the circuit. After the object camera shutter was opened, the variac switch was closed and immediately opened. The resulting instantaneous current was sufficient to detonate the charge. The leads from the safety switch were passed up the side of the blast table frame and through the copper tube to the charge.

E. Basic Electronic Circuit. (See Fig. 6)

Photocell #1 was supported directly below the hole in the center of the blast table. To provide continuity in the blast table, so that the hole would not interfere with the reflected shock front, a lucite rod was placed up through the hole until it was flush with the top surface of the blast table. The rod also prevented unexploded PETN particles, resulting from low order detonations, from entering the photocell. The rod extended down into the photocell terminating slightly above the phototube. With this arrangement the photocell could sense the explosion of the charge without interfering with the shock front.

The delay generator was positioned well behind the microflash unit and in close proximity to the CRO and electronic counter. The lead from photocell #1 was connected to the "PFR Drive" connection of the delay generator. The following positions and settings of all electronic components were not in accordance with the preliminary set-up procedure found in the applicable instruction manual.

The positions and settings for the delay generator were:

- (1) triggering level knob - orange dot in "1030" position and white arrow on "positive going - AC".
- (2) sweep trigger switch on "direct".

The output from the delay generator came from the "delayed sync. out" connection and went to the power unit of the microflash. This unit was best positioned on top of the delay generator. The power unit was removed from its case so that its input from the delay generator could be connected directly across the microphone receptacle, S02, (refer to wiring diagram of microflash manual). The voltage to fire the flash was passed from the power unit to the lamp unit using the high voltage cable provided with the microflash unit. Extreme caution was exercised in making the above connections and in manipulating the microflash unit since the power and lamp units contained voltages up to 1500 and 8500 volts respectively.

The signal from photocell #1 was also connected to the "start input" receptical of the electronic counter. This signal started the counter counting in tenths of microseconds. The important positions and settings for the counter were:

- (1) Sep-Com switch to "SEP"
- (2) Start and stop trigger slope to "+"
- (3) Start and stop trigger level voltage to "8x3"
- (4) Display time knob to the 12 o'clock position

Reliable operation of the electronic counter could only be expected after a warm up time (master switch to "on") of a minimum of two hours. The counter was left connected to the wall outlet with the master switch in the down position at all times when not in use. This provided continuous heating of the counter.

Lastly the signal from photocell #1 also went to the "external trigger in" connection of the CRO. For operation of the CRO the positions and settings were:

- (1) trigger: slope switch to "+", coupling switch to "AC", source switch to "ext."
- (2) sweep time/cm variable switch to calibrated position (full clockwise).
- (3) vertical sensitivity to 20 v/cm.
- (4) AC-DC-Gnd switch to "DC".

The flash of the microflash was sensed by photocell #2 which was mounted on a movable ring-stand adjacent to the lamp unit of the microflash. A small hole was cut through the aluminum foil at one edge of the lamp face through which the photocell could see the flash. This hole was shielded so that the light from it would not directly illuminate the reflective screen. It was determined that for best results in stopping the electronic counter, the end of the photocell should be placed one inch from the lamp face.

The signal from photocell #2 was supplied to the stop input connection of the electronic counter to stop the time measurement and leave the exact elapsed time between explosion and light flash displayed on the counter in tenths of microseconds. The only error that could be present in this time display was the error internal to the electronic counter itself and the error introduced in the time it would take for the output signal from the photocell to build up to the threshold voltage required to actuate the electronic counter. The former was eliminated by ensuring through calibration that the error was within the design limits of \pm one microsecond. The latter error was determined to be one

to two microseconds. This was accomplished by supplying a signal from the photocell simultaneously to the trigger circuit and vertical deflection circuit of the CRO. The photographs of the CRO traces showed clearly a rise time of the photocell signal of one to two microseconds.

The true time interval as displayed on the electronic counter was, therefore, accurate to \pm three microseconds. This time, however, was consistently 35-40 microseconds greater than the time set on the delay generator dial. This error was either in the delay generator or the microflash unit. By connecting the CRO across the input and output of the delay generator, its error was determined to be within the design limits of one percent of the dial setting. The delay between the input signal to the microflash power unit and the flash of the lamp varied from 35-40 microseconds. This was determined by supplying the output from the delay generator simultaneously to the power unit and to the trigger input of the CRO. A photocell was positioned to sense the flash and to provide its signal to the vertical sweep of the CRO. The time delay was read from a photograph of the resulting CRO trace.

The signal from photocell #2 was also supplied to the vertical sweep connection of the CRO. When this impulse was received by the CRO it was registered on the cathode-ray tube. This trace which was initiated as a horizontal line at the time of explosion and distorted vertically at the time of light flash was recorded on the film of the CRO camera. The time was read from this film to an accuracy of about two percent. It was therefore merely used as a cross check for the electronic counter.

F. Camera and Lamp Unit: (See Fig. 4)

The position of the camera was varied depending on the area of the shock front that was of primary interest. For the initial pictures

of the primary shock front the camera was placed directly beside or above the lamp unit. This was satisfactory for the preliminary qualitative work since it was desired that the picture include the entire shock front for all time delays. However, to make more accurate measurements of the shock front radius the camera should be moved as close to the screen and charge as possible without interfering with the shock front or casting shadows on the screen. To eliminate shadows, the camera was moved to one side of the center line. This position proved unsatisfactory due to the interference of the bright reflection of the explosion. In an attempt to move this reflection where it would not interfere, which was to the point on the screen directly behind the charge, the camera was positioned on the centerline but above the horizontal line from the light source to the charge. This was accomplished by suspending the camera below a tripod. The legs of the tripod were extended so that they did not cast shadows on the area of interest. The height of the camera was varied so as to keep it as low as possible which would keep the explosion reflection low but yet not cast its own shadow on the area where the shock front was expected to appear. It should be remembered that the position of the shock front on the film is completely independent of the position of the camera since the camera is photographing the shadow of the shock front on the screen and not the shock front itself in the plane of the explosion. It should be pointed out that the field of view of the camera need not include the center point of the blast on the screen due to the method used to measure the shock front radius. This will be discussed in a later section.

The optimum position of the camera then, for the first set of photographs in which the primary shock front was of interest, was

horizontally on the center line but above the charge and approximately three feet from the screen.

It was found that for the measurement of the Y-stem data the camera should be moved to one side slightly to give a better view of the Y-stem area and yet not move the blast reflection into the area of interest. Close-up photography of the Y-stem formation was attempted with the use of attachable close-up camera lenses. For these close-up photographs the camera was moved into approximately 24 inches from the screen. Some usable pictures were obtained, but the most well defined shock front images were obtained at the cameras minimum distance of three feet without the use of close-up lenses.

In order to make the microflash essentially a point source of light, the face of the lamp unit was covered by a square piece of aluminum foil with a one centimeter hole cut in its center. A point source light ensured that the shadow of the shock front was narrow and well defined.

The lamp unit was placed horizontally in a direct line with the charge and the center grid of the reflective screen and vertically so that the light aperture was the exact height of the charge. This position facilitated the measurement of the primary shock front radius. The lamp unit was lowered so that the aperture was level with the blast table when the formation of the Mach Y-stem was investigated. This was necessary so that the shadow of the Y-stem would be projected onto the reflective screen rather than onto the blast table.

The distance of the lamp unit from the screen was varied to determine the optimum distance for the sharpest shock front. It was first thought that this would be accomplished if the light beams were parallel, that is, the lamp placed at an infinite distance. This distance was simulated by placing the lamp unit the maximum distance

away possible, 18 feet, with negative results. The next position tried was 300 cm. This position was still not satisfactory and the 200 cm position was tried. Some good shock waves were photographed at this distance but the pictures were too small for accurate measurements. It was decided to move the entire set-up closer to the screen. The blast table was moved in flush with the screen which made the charge 41.5 cm from the screen. The light was placed at 109 cm and the camera was placed at three cm. At this light distance the shock wave appeared fuzzy even though the grid screen was in sharp focus. Therefore, the light was moved back to 165 cm. Good definition of the shock wave was obtained at this distance.

3. Preparation of charges.

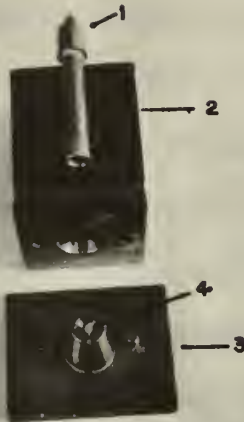
In preparing the charges for the experiment, a steel die was obtained from the Explosives Laboratory which would compress about 250 mg of pentaerythritol tetranitrate, PETN, around an approximately 55 mg detonator. The diameter of the bowl of the die, see Fig. 7, was .75 cm which resulted in a spherical charge of .225 cc. The loading density was 1.5 grams/cc.

A charge was prepared by cutting a 15 cm length of nichrome fuze wire in which an overhand knot was tied and adjusted so as to be in the center of the wire. This length of wire weighed 25 mg. The knot was pulled tight enough so the loop was one mm in diameter. This knot was necessary to give a base for the application of the rest of the detonator.

Lead styphnate was used as the first layer of the detonator because of its high sensitivity to heat. The lead styphnate was mixed with a small amount of Duco cement and acetone. After thorough mixing and when some of the acetone had dried to obtain the proper consistency, a small drop of the mixture was applied to the knotted fuze wire. When the acetone completely dried, the lead styphnate bead, with the glue binder, adhered to the fuze wire and was ready for application of lead azide. However, if insufficient glue was used, the resulting styphnate bead would flake away or break apart in subsequent handling. Too much glue led to low order explosions, therefore, the minimum amount of glue was used to adequately bind the styphnate. The total amount of glue and styphnate used averaged five milligrams.

A layer of shock sensitive lead azide was applied around the styphnate bead using the same mixing procedure as before, only, due to

Charge Die and Press



- 1. Plunger
- 2. Die Top
- 3. Die Base
- 4. Detonator

Figure 7a



- 1. Press
- 2. Glass Funnel
- 3. Spatula
- 4. Metal Rod
- 5. Pliers
- 6. Die Top
- 7. Plunger
- 8. Completed Charge and Detonator
- 9. Die Base
- 10. Allen Wrench

Figure 7b

the cohesive nature of the azide itself, very little glue was required. Approximately 25 mg of lead azide was used which made the total detonator weight approximately 55 mg. Since the fuze wire weighed 25 mg, the explosive portion of the detonator weighed 30 mg, only 8% of the entire explosive charge.

It should be noted that in the preparation of the detonators, actual weighing of each component used was not necessary. Of the completed detonator, the weight of wire (25 mg) was fixed. The remaining portion of the detonator was mostly lead azide. So little sytphnate was used that its weight varied only within one milligram. With the weight of these two components constant, the azide was applied until the total detonator weight exceeded 55 mg. This final desired weight was used due to the high incidence of low order explosions from previous charges when detonators weighed from 35 to 45 mg. With practice this final weight of 55 mg was obtained with very small error.

The PETN charge itself was made by capsulating the detonator inside the 250 mg of PETN and compressing it in the die. The PETN was donated by the Trojan Powder Company of Allentown, Pennsylvania. Since it was stored under water, it required being dried for about three hours with occasional stirring. If heated excessively it was noted that the PETN turned light yellow. The use of this PETN led again to low order explosions.

Once dried, the powder was stored in a dessicator and only left exposed to the atmosphere long enough to prepare a series of ten to twenty charges at a time. Occasionally, low order explosions occurred which were due, in part, to the hygroscopic property of PETN.

The method of capsulating the detonator in the PETN was as follows:

a. 285 mg of PETN was accurately weighed out. The use of the Mettler type balance greatly decreased the time required to make these weighings.

b. The upper and lower sections of the die were placed together and about one-third of the PETN was poured into the bowl of the die. A small funnel was used to keep spillage at a minimum. The PETN was tamped down lightly in the bottom of the bowl. (A SAFETY FACE MASK WAS ALWAYS WORN DURING THIS OPERATION)

c. The upper section of the die was removed. No PETN was spilled if the preceding operation was done carefully. The fuze wire was crimped on both sides of the detonator so that a right angle was formed. The wire ends were inserted through the small holes located on each side of the bowl pedestal and pulled, from the bottom, until the detonator rested on the partially filled bowl. It was necessary to ensure that the wires laid in the grooves provided so the upper section of the die was able to slide down snugly over the pedestal.

d. When the upper and lower half were again placed together, the remaining PETN was poured into the bowl and the plunger inserted. The die and plunger were now placed in the press and the press screwed down until hand tight. If too much pressure was applied the plunger struck the metal bowl and became belled-in. This required either remachining or reforming, using a small ball bearing. Also, excessive pressure caused the plunger to sever the fuze wire. The die was left in the press approximately one minute.

e. Upon releasing the screw pressure and removing the plunger and upper section of the die, the fuze wires were pulled out of the pedestal

base holes. Due to the adhesion between charge and bowl, the charge was then released by raising slightly the small brass plunger which protruded through the bowl pedestal. This was done by turning a small hex-screw on the bottom of the die. Then the charge came out freely.

f. The completed charge was accurately weighed to ensure that the total weight was 250 mg plus the weight of the detonator. The weight was usually accurate within 5 mg. If the charge weight exceeded the desired weight a spatula was used to scrape the excess PETN from the charge. If the weight was only slightly less than that desired, the charge was used but its actual weight was recorded.

This procedure worked quite satisfactorily but was perfected only after considerable effort was spent on (1) trying to break the adhesion between charge and bowl without losing portions of the charge and thereby ruining its spherical geometry and (2) trying to eliminate the spillage which resulted when pressure was applied to the plunger.

In an attempt to eliminate the first problem, liquid graphite and liquid mold release was sprayed on the bowl and allowed to dry. The application of both failed to release the charge satisfactorily. Finally, by enlarging the diameter of the brass plunger seated in the bowl, the complete charge came out as described in paragraph (e) above.

The problem of spillage was never eliminated, although the volume of the cavity in the plunger was enlarged and the knife edges of the plunger were made sharper, in hopes that the entire quantity of PETN would be compressed around the detonator with the minimum spillage. Spillage, however, could not be eliminated with the existing die and, therefore, to obtain consistently 250 mg of PETN the problem was circumvented by adding excess PETN. By trial and error it was determined

that 35 mg excess was necessary to consistently obtain 250 mg of PETN in a completed charge. The spillage had to be cleaned from both sections of the die prior to preparing another charge.

4. Experimental Procedure

Prior to firing a series of charges, all electronic equipment was energized for a minimum of two hours. After the prescribed warm-up period, the electronic counter was checked for timing accuracy by switching the Function Selector to "100 KC CHECK" and then to "10 MC CHECK". With the Function Selector in each position, the Frequency Unit Switch was cycled through the five positions of frequency. At each frequency the counter column corresponding to that frequency should register 1.000. If not, the counter required further warm-up.

The oscilloscope was checked to ensure that the "Sweep Time/Cm" was at the proper position to ensure maximum use of the entire scope face for the prescribed delay time. This was desirable to give the greatest accuracy in reading the delay time from the CRO picture. The "DC BAL" was calibrated as per CRO 504 instruction manual. In addition the horizontal position was checked to ensure that the trace started exactly at the left edge of the grid. This was accomplished by viewing the CRO as a test light was manually passed across photocell #1, thereby producing a test trace. The test light procedure also provided a check that there were no open circuits since it also initiated the microflash. It must be recognized, however, that the trace time did not correspond to the delay set into the delay generator. This error was caused by the long duration of exposure of the test light to photocell #1. At times, the manual sweep test did not initiate the microflash even though the microflash circuit was complete. In these cases, the sensitivity to the microflash power source required adjusting or the internal circuitry of the delay generator required cycling. This was done by turning the RESET switch to "SWEEP" and then back to "DELAY"

several times. This problem, however, was not encountered when photo-cell #1 was initiated with the explosive charge.

Since the blast table, microflash, and cathetometer could have been moved inadvertently since the last series of firings, the prescribed distances of each unit from the reflective grid screen were checked as well as the level of the blast table.

The oscilloscope camera and the object camera were loaded with new film, if needed, and the focus and lens aperture of the object camera were adjusted.

After the above procedure was completed, the charge was attached to the firing circuit leads, after first ensuring that:

- (1) the variac switch was off,
- (2) the safety switch was open,
- (3) A FACE MASK WAS WORN.

The charge was then connected to the leads by twisting the charge wire ends around the leads sufficiently to provide electrical continuity and so the charge would not fall off during positioning.

To accurately position the charge, it must be moved about in the plane of the charge holder until the crosshairs of the cathetometer, the charge itself, and the bench mark on the reflective grid screen were all in line.

Once the charge was in position, the object camera was cocked, ensuring the exposure time setting was on "B", and the safety switch closed. The variac was set at 60 volts. The room was darkened and the apertures of both cameras were opened. A warning buzzer was actuated for five seconds and then the variac switch was cycled to "on" and immediately back to the "off" position. This action detonated the charge.

Immediately after the explosion, the apertures of both cameras were closed, the safety switch opened and the room lights turned on. An estimation was made at this time as to the order of the explosion. If the exploding charge seemed to spark, as in Fig. 8 or if the sound was not of high intensity, or if small particles of PETN were found on the blast table, these symptoms indicated a low order, incomplete explosion. However, if the sound of explosion was loud and sharp, and a sphere of quickly disappearing exploding gas was observed, and there was no evidence of unexploded PETN, this was a good indication of a high order explosion.

The electronic counter reading and any of the above symptoms, if pertinent, were recorded. The time interval as shown on the CRO film was also recorded. In this manner a set of three times were obtained: the delay time set, the counter time, and the CRO time.

Usually, the series of charges were detonated in rapid order. For subsequent firings, it was only necessary to reset the counter, check the cameras, dial a new delay generator setting, and attach another charge.

At the completion of the series, all equipment was de-energized, except the electronic counter which was always left plugged in but with power off, thereby allowing the counter heater to maintain its internal circuitry at a constant temperature.



5. Data

The following procedure was used to obtain usable data from the object camera photographs.

After the polaroid film was treated with preservative and allowed to dry it was mounted on a traveling microscope obtained from the USNPGS Physics Department. However, magnification was too great to enable the shock front to be distinguished from the background. Since these were the only microscopes available and there were no interchangeable eye pieces or objective lenses available with a lower magnification, a negative lense was attached by small pieces of wax directly below the objective lens, thereby decreasing the magnification of the film and rendering the shock front visible.

The following data was measured from the photographs and recorded; the primary shock front radius, R_p ; the height of the triple point, H_{tp} ; the horizontal distance of the triple point from ground zero, D_{tp} , and the horizontal distance of the Y-stem from ground zero, D_y . (Table 1)

The best accuracy in the determination of this data was obtained when measurements were made to give the proportion of the distance between the two adjacent grid lines between which the shock front was observed. The number of whole grid squares from the blast wave to the projected point of explosion were then added to this distance obtained from the measured ratio. As an exemple, assume the shock front radius was approximately 48 cm. The only measurements taken from the photographs were the distance from the fourth grid line to the shock front and the distance from the fifth grid line to the shock front. This ratio of distances was multiplied by 10 cm and then added to 40 cm to

give the actual radius of the shadow of the shock front. This method of measurement was the most accurate since the camera could be positioned close to the grid screen so that the distance to be measured included the maximum area of the film. In fact, this method was mandatory for accuracy in the long delay time, large radii explosions due to the foreshortening of the grid squares on the film. This error was considerable for radii larger than 30 cm. The vertical foreshortening of the grid square being measured was virtually eliminated by adjusting the height of the camera to approximately that height at which the blast wave was expected to appear.

The distances obtained thusly for R_p , H_{tp} , D_{tp} , D_y , were the distances for the shadow of the shock front on the grid screen. These distances were divided by the appropriate geometric factor to obtain the magnitude of the parameters in the actual shock front. The geometric factor is dependent only on the distances between source light, charge and grid screen. The calculation of this factor is shown for the last physical set-up used. A side-on view of the physical set-up is shown;

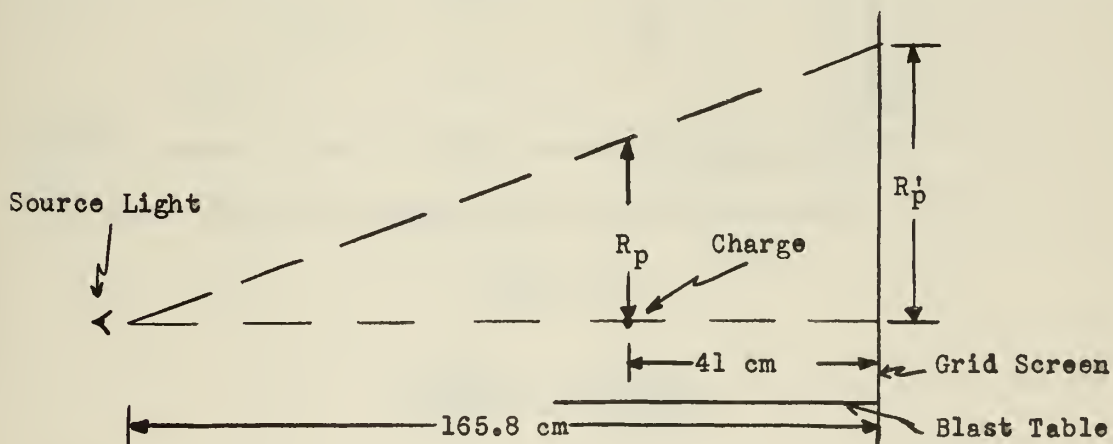


Figure 9

From this diagram:

$$\frac{R_p}{165.8 - 41} = \frac{R'_p}{165.8}$$

$$R_p = \frac{R'_p}{165.8/124.8}$$

therefore, the geometric factor, $f = \frac{165.8}{124.8} = 1.33$

This factor applies to R_p as well as to D_{tp} , and D_y when the light was positioned level with the charge. A slightly different form of the ratio was used for H_{tp} , since it was measured from the blast table to the Mach Y-stem.

When the source light was placed level with the blast table the following diagram and ratio were applicable for R_p . A simple ratio similar to that shown above was used for H_{tp} , D_{tp} and D_y .

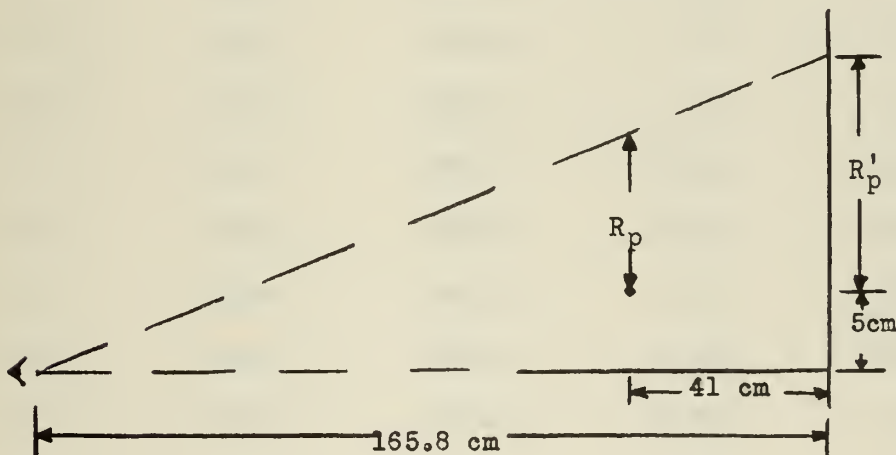


Figure 10

$$\frac{R_p + 5}{124.8} = \frac{R'_p + 5}{165.8}$$

therefore,

$$R_p = \frac{R'_p}{1.33} - 1.24$$

TABLE I

Omissions in the table are due to those parameters not being of main interest and, therefore, not in the field of view of the object camera. Shots prior to #142 were for $h=5$ cm and those following #142 were for $h=8$ cm.

| <u>Shot No.</u> | <u>R_p</u> | <u>t</u> | <u>H_{tp}</u> | <u>D_{tp}</u> | <u>D_y</u> |
|-----------------|-------------------------|-----------------------|----------------------------|----------------------------|-------------------------|
| 1 | 19.26 | 245.4 | 7.32 | 20.17 | 21.38 |
| 3 | 19.84 | 242.8 | 5.44 | 19.96 | 20.71 |
| 4 | 19.62 | 244.3 | 6.56 | 19.37 | 20.17 |
| 6 | 19.55 | 242.2 | -- | 18.54 | 20.23 |
| 7 | 19.71 | 241.8 | 6.89 | 19.37 | 20.44 |
| 10 | 17.85 | 194.2 | 6.29 | 16.81 | 17.80 |
| 12 | 22.80 | 291.9 | -- | -- | -- |
| 13 | 22.75 | 295.9 | 8.77 | 21.52 | 22.70 |
| 14 | 11.47 | 84.9 | -- | -- | 10.54 |
| 15 | 16.40 | 165.7 | -- | -- | 14.52 |
| 17 | 24.00 | 340.0 | 10.12 | 23.16 | 25.28 |
| 18 | 29.70 | 448.2 | 15.23 | 26.63 | 32.46 |
| 19 | 33.60 | 545.4 | 16.76 | 30.55 | 34.96 |
| 20 | 39.20 | 646.8 | 23.00 | 32.63 | 39.92 |
| 21 | 43.00 | 744.6 | 22.20 | 37.88 | 41.96 |
| 23 | 14.70 | 133.5 | 4.06 | 13.45 | 13.99 |
| 25 | 14.70 | 133.2 | -- | -- | 13.45 |
| 27 | 14.00 | 128.0 | -- | -- | -- |
| 39 | 21.3 | 265.0 | -- | 19.90 | 20.98 |
| 40 | 19.25 | 185.0 | -- | -- | -- |
| 105 | -- | 102.0 | 2.80 | 11.52 | 12.38 |
| 113 | -- | 88.0 | 2.18 | 10.29 | 10.64 |

| <u>Shot No.</u> | <u>R_p</u> | <u>t</u> | <u>H_{tp}</u> | <u>D_{tp}</u> | <u>D_y</u> |
|-----------------|----------------------|----------|-----------------------|-----------------------|----------------------|
| 120 | -- | 69.6 | 1.14 | 9.14 | 9.14 |
| 123 | -- | 75.0 | 1.23 | 9.81 | 9.95 |
| 124 | -- | 74.0 | 0.59 | 10.29 | 10.29 |
| 125 | -- | 73.1 | 1.19 | 10.08 | 10.29 |
| 127 | 10.76 | 80.9 | 1.43 | 10.68 | 10.66 |
| 133 | 10.82 | 83.4 | 1.75 | 10.29 | 10.71 |
| 135 | 11.69 | 88.0 | 1.75 | 10.24 | 10.41 |
| 137 | 12.26 | 89.0 | 2.13 | 10.22 | 10.49 |
| 138 | 12.40 | 95.0 | 2.17 | 11.22 | 11.52 |
| 142 | 14.78 | 144.1 | 1.12 | 12.91 | 12.72 |
| 144 | 15.45 | 151.5 | 0.63 | 13.04 | 13.04 |
| 145 | 16.22 | 164.0 | 2.30 | 13.98 | 14.58 |
| 146 | 16.72 | 173.3 | 1.86 | 14.69 | 15.03 |
| 151 | -- | 279.5 | 2.29 | 21.08 | 21.09 |
| 152 | -- | 331.0 | 3.09 | 23.07 | 23.16 |
| 154 | -- | 381.0 | 4.67 | 26.38 | 26.73 |
| 155 | 18.94 | 231.0 | 2.26 | 17.44 | 17.51 |
| 156 | 19.11 | 211.0 | 2.15 | 17.32 | 17.52 |
| 157 | 16.56 | 171.0 | 1.86 | 14.64 | 15.03 |
| 158 | 14.87 | 147.1 | 0.65 | 13.39 | 13.63 |
| 159 | 15.73 | 156.0 | 1.13 | 13.79 | 13.79 |
| 162 | 17.43 | 190.0 | 2.24 | 15.85 | 15.85 |
| 163 | -- | 252.0 | 2.71 | 19.08 | 19.08 |
| 167 | -- | 285.0 | 4.24 | 20.54 | 20.84 |
| 168 | -- | 325.0 | 4.68 | 22.02 | 22.02 |
| 169 | 19.31 | 225.0 | 2.36 | 17.81 | 17.81 |
| 170 | 15.90 | 162.0 | 0.93 | 13.45 | 13.45 |

6. Calculations

Several correlations and calculations were determined from the data obtained from the photographs. The most important of these were:

- (1) the Mach number, M , from which the overpressure was calculated,
- (2) the angle of incidence of the shock front when the Mach Y-stem initially formed,
- (3) the scaled distances and scaled time,
- (4) and the determination of the average yield of the PETN charge.

To eliminate the possibility of human error in the many repetitive calculations described below, a Computer Data Corporation Model 1604 computer was utilized. The program used is described in Appendix I.

A. Mach Number

The Mach number is the ratio of the shock wave velocity to the velocity of sound. Thus, a relationship between distance, time and M was obtained,

$$M = u_x/a = \frac{dR_p/dt}{dR_p/dt_a}$$

or

$$M dt = dt_a$$

but

$$dt_a = dR_p/a$$

therefore

$$dt = dR_p/Ma$$

by subtracting, we have

$$dt_a - dt = \frac{R_p}{a} \left(1 - \frac{1}{M} \right)$$

or

$$M = \frac{1}{1 - a \left[\frac{d(\Delta t)}{dR_p} \right]} \quad (1)$$

where

$$\Delta t = dt_a - dt$$

The quantity dt/dR_p is simply the slope of the curve resulting from a plot of Δt versus R_p . To obtain this slope, the equation of the best curve through the Δt and R_p data first had to be determined. (See Fig. 11) The computer gave a set of polynomials from first order to sixth order which gave the best fit with experimental data. By comparing the curves of these polynomials with the experimental curve it was determined that the fourth order curve most closely agreed with the experimental data. The equation of the fourth order curve used is:

$$\Delta t = -1.488 + 30.204 R_p - .9657 R_p^2 + .01889 R_p^3 - .00015 R_p^4 \quad (2)$$

By differentiation of equation (2), the equation of the slope of this curve was determined and utilized by the computer to give the slope at any point on the curve. This equation is:

$$\text{slope} = 30.204 - 2(.9657)R_p + 3(.01889)R_p^2 - 4(.00015)R_p^3 \quad (3)$$

By substituting the calculated slope for various values of R_p in equation (1), the Mach number was calculated. The overpressure was then calculated using equation (4).

$$p = \frac{7}{6} (M^2 - 1) P_0 \quad (4)$$

where P_0 is the atmospheric pressure.

B. Angle of incidence

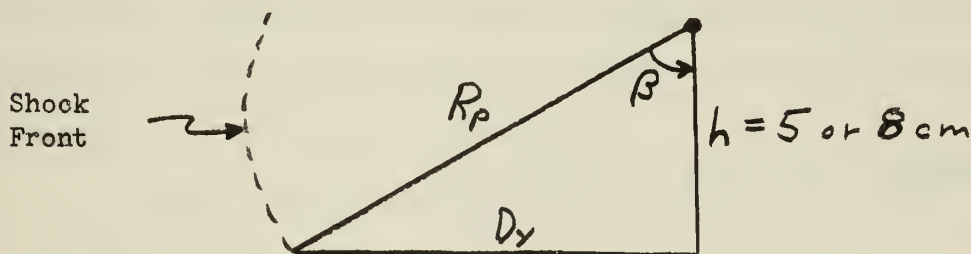
To calculate the angle of incidence, β , it was necessary to determine the time at which the Y-stem began to form. This was done by using the data from a series of close up photographs with small delay time settings. When the data from these shots was incorporated with previous data, a smooth curve of height of Y-stem, H_{tp} , versus time resulted. (See Fig. 12) By extrapolating this curve to zero height, the time of Mach Y-stem formation was determined. For a height of charge, h , equal to five cm the time was 60 microseconds. For a height of charge equal to eight cm the time was 135 microseconds.

Using these times, the angle of incidence was calculated by two methods. The first method incorporated the interpolation between experimental points of R_p and t to determine R_p for 60 microseconds and 135 microseconds. This interpolation gave values of 8.87 cm and 14.3 cm, respectively, for the radius of the primary shock front at the time of Y-stem formation. Then,

$$\beta = \cos^{-1} h/R_p$$

For the second method, the horizontal distance from ground zero to the Mach Y-stem, D_y , was obtained from the D_y versus t plot at the appropriate times. (See Fig. 13) For $t=60$ microseconds, $D_y=8.8$ cm and for $t=135$ microseconds, $D_y=12.5$ cm. Then,

$$\beta = \tan^{-1} D_y/h$$



By method (1), β is 54.9° and 56° for 5 cm and 8 cm, respectively.

By method (2), β is 60.2° and 57.4° for 5 cm and 8 cm, respectively.

C. Scaled Distance and Scaled Time

Scaled distance and scaled time were required for correlation of the experimental data with data for any other reference explosion. The effects of an explosion vary with the intensity of the blast and with the density of the transmitting medium. Since the effect is spherical or volumetric a cube root scaling law was used.

The scaling law for distance is:

$$\text{scaled distance} = \frac{f_d (\text{actual distance})}{\omega} \quad (5)$$

where f_d = transmission factor for density $= \left(\rho/\rho_0\right)^{\frac{1}{3}}$ and ω = yield factor $= \left(\frac{W}{W_0}\right)^{\frac{1}{3}}$

Since the experimental and reference data was obtained at sealevel, $\rho = \rho_0$ and f_d is equal to unity. W_0 is the yield of the reference explosion and is equal to one ton of TNT at 70° F. The average experimental temperature was 71°F. This difference was considered negligible and 70°F is used throughout the calculations. To determine the average yield per charge, W , in TNT equivalents, the following basic data was compiled:

Average weight of PETN per charge = 249 mg

Average weight of lead azide and lead styphnate per charge = 30 mg

The equivalents of the above explosives to TNT are 173%, 40%, and 39%, respectively. (Reference 1) Using a weighted average for the TNT equivalents for lead azide and lead styphnate of 39.2%, the total equivalents of PETN/charge was calculated.

$$W = 249 + 30 \left(\frac{.392}{.173} \right) = 255.8 \text{ mg PETN/charge}$$

or in units of tons of TNT,

$$W = \frac{.2558 \times 1.73}{453.6 \times 2000} = 4.89 \times 10^{-7} \text{ tons TNT/charge}$$

and,
$$\omega = (4.89 \times 10^{-7})^{\frac{1}{3}} = .00787$$

The time scaling law is;

$$\text{scaled time} = \frac{f_d \times f_a \times (\text{actual time})}{\omega} \quad (6)$$

where f_d and ω are defined above. f_a is the transmission factor for the speed of sound and is equal to $\left(\frac{a}{a_0}\right)$. This ratio is proportional to the square root of the temperature ratio, therefore, f_a also is equal to one.

D. Average Yield

The scaling law for distance shown above (Eq. 5) can be used in an inverse way to determine the average yield of explosive charge. The average yield was calculated to ascertain if the experimental data did, in fact, correspond to the known yield of 255.8 mg PETN equivalent. The equation in the proper form is;

$$W = W_0 \rho_d^3 \left(\frac{\text{Actual distance}}{\text{scaled distance}} \right)^3$$

where all symbols are defines as above.

The distance ratio used in Eq. 7 was determined by two methods:

(1) Visual weighing of the experimental data using plots of b ratio versus the log of distance for the experimental and reference explosions.

(2) Analytic determination using the distance - arrival time ratio, b, to select a scaled distance.

Each method was calculated assuming a point source explosion. This assumption is justified since the shock front radius data exceeds ten times the charge diameter after which the effect of the displacement of the atmosphere by the explosive charge mass is considered negligible.

Method (1), as described in reference 2, is the correlation of b ratio with actual distance and scaled distance. In this method calculated b ratios were plotted on the ordinate and the log of distance in centimeters was plotted on the abscissa. A similiar plot, using the b ratio data from a reference explosion of one ton of TNT (Table 11 of Reference 2) and the corresponding scaled distance in feet was made. The two plots were then placed on top of each other, so that lines of equal b ratio remained superimposed. The two graphs were moved horizontally until the curves agreed as closely as possible.

The actual distance in centimeters and the scaled distance in feet corresponding to this point of intersection were then read from the respective abscissa. The two distances are corresponding distances representing equal b ratio for the two explosions. Incorporating these two distances in equation (7), resulted in a average yield of 275 mg of PETN. Figure 14 shows these two plots on one graph superimposed to give the best fit.

Method (2), also outlined in reference 1, used the raw data directly to obtain the b ratio. The b ratio is tabulated in reference 2, in feet per millisecond and thus required conversion of R_p from centimeters to feet and t from microseconds to milliseconds. The simple but tedious calculations were also programmed and printed by the computer. By entering Table 11 with the b ratio, a scaled distance in feet was obtained. This distance was the distance corresponding to R and resulted in a surprisingly increasing trend in yield when calculated by equation (7). (See Fig. 15) However, when yield is extropolated to zero distance, a value of 212 milligrams is obtained. This trend is discussed in the next section.

E. Data Correlation

To correlate the data obtained with that from larger scale explosions, certain calculations were necessary. The basis for these calculations is the energy of explosion, ΔA , of PETN. ΔA has been calculated for PETN to be 7.69×10^{10} ergs per gram. For the size charges used, 255.8 mg, ΔA is 1.91×10^{10} ergs. Using the $1/3$ power scaling law a reduced energy parameter, α , in centimeters, was calculated.

$$\alpha = (A/P_0)^{1/3} = 26.79 \text{ cm}$$

A reduced radius parameter, λ , and reduced time parameter, τ , were also calculated,

$$\lambda = \frac{R_p}{\alpha} \quad \text{and} \quad \tau = \frac{at}{\alpha}$$

7. Conclusions

The shock front photographs were excellent for the purpose of recording the primary shock front and the Mach Y-stem data. It was observed that at low time delay settings, the reflected front could not be seen due to the expanding gases of explosion. At larger time delays, the reflected front was well beyond these gases and was readily observed. Occasionally a portion of the secondary shock front was observed. This shock front follows a rarefaction wave into the PETN gases. It starts with zero strength and grows as it moves inward through these gases. It is swept outward in space until the expansion of the high explosive products is nearly exhausted, and then it implodes on the origin and is reflected outward to the contact surface. At the time it strikes the contact surface between the PETN gases and the air, the PETN gases are still more dense and much cooler than the air immediately outside, (this is generally true at any time). As a consequence, the shock in passing through the surface sets up an inward rarefaction wave. This rarefaction, like the initial rarefaction, is followed by a third shock front moving inward. This shock, like the second implodes on the origin, reflects and moves out in the wake of the previous shocks. The succession of shocks continues in this manner until the energy in the explosion product gases is dissipated. (see Ref. 3) The third and succeeding shock fronts were not observed. Figure 16 is included from Reference 3 to show the position of the shock fronts described above as a function of time.

The delay times recorded from the electronic counter were, as stated in Section 2, accurate to \pm three microseconds. Therefore, the basic data R_p and t , used in arriving at the conclusions

described below is considered a true representation of the actual experimental phenomena observed.

A. Correlation with high yield explosions

One avenue of interest pursued was to determine how close the experimental data from the decigram charges of PETN correlated with the data from one ton of TNT. If the correlation was close, the feasibility of using laboratory scale explosions instead of tons of high energy explosives at a remote test site to simulate the latter would be proved.

Of primary concern in judging the effectiveness of an explosion is the peak overpressure, ΔP , at a given distance from the explosion. Figure 17 is a plot of the log of the overpressure versus the log of the reduced radius, λ . The experimental data obtained for PETN is compared to the theoretically calculated data for TNT obtained from Brode (Reference 3). As can be seen, the correlation is quite good for the low values of λ . At large reduced radii, the overpressure is greater than that indicated by the point source, ideal gas curve. This ideal gas curve defines the maximum overpressure for a given radius, since for an explosion in real air the molecular dissociation and ionization of the explosive gases at high temperatures reduces the blast efficiency. The discrepancy is due to experimental error at large radii and can be explained thusly: The light from the micro-flash cast a shadow of the point on the surface of the spherical shock front that is tangent to its path. At low radii this point is in the vertical plane through the point of explosion. But as the shock front radius increases this tangent point moves out of the plane of the charge and toward the light. By simple geometric construction

it can be seen that this will give an apparently larger radius.

Figures 18 and 19 of reduced and scaled parameters, respectively, also show good correlation with TNT data from References 2 and 3.

B. Comparison of known yield with calculated yield

The result of the yield calculations, although not consistent for each method used, gave a calculated yield of the same order of magnitude, 275 mg and 212 mg. The per cent error from the known value of 255.8 mg of the two methods was 7.5% and 13.2% respectively.

The first method of calculation as discussed in Section 6 is considered more direct and by superpositioning of the two curves (Fig. 14) many experimental uncertainties are minimized. For this reason, more credence is given to the value of 275 mg.

The linear increase of yield obtained in the second method resulted from experimental error which is a function of increasing R_p . This method of yield determination should give a horizontal straight line at a constant yield of 255.8 mg. The positive slope of this line is contrary to physical fact. The random error due to small variations in charge size and positioning, etc. will fluctuate somewhat, but should give an average around a constant yield. By extrapolating the curve obtained to zero radius it can be assumed that the experimental error, which is a function of R_p , has been minimized and therefore the value of 212 mg of PETN is obtained.

The sources of the experimental error were considered to be a combination of several factors, but after considering each factor, all except one were discarded.

The most probable error considered was time error. However, after a careful investigation of the error across all electronic

components with the CRO, as described in Section 2, the unaccountable error was determined to be \pm three microseconds. This source of error was therefore eliminated.

The buckling of the blast table was considered. Although some buckling was possible, it was considered extremely small due to the lab jack supports located directly under the area of the blast table from which the front was reflected. However, any buckling would be due to the absorption of energy from the shock front system and hence tend to decrease the calculated yield. This factor, therefore, has the reverse effect on yield as that observed and was eliminated.

Another source of error considered was the variation in atmospheric conditions and charge weight. But, the atmospheric conditions were relatively constant. The variation of charge weight, although small, could possibly have caused an increase in yield of the weights increased with an increase in delay times. However, the selection of charges was completely random and any error due to this variation would have cancelled out.

The one possible error which did effect yield with an increase in R_p was the geometric factor error as discussed above. This error resulted in R_p 's greater than actual. When inserted into Equation 7, it has the effect of increasing the numerator and decreasing the denominator since the scaled distance varies inversely with the b ratio. This term is then cubed which greatly magnifies this error. Therefore this error is a function of R_p . By extrapolation to zero R_p , it is assumed that the effect of this error is minimized.

The values of 275 and 212 mg of PETN yield are considered good due to the inherent random nature of experimental explosive research.

C. Angle of incidence for Mach Y-stem formation

Another avenue of interest was verification of the angle of incidence for the formation of Mach Y-stem. From reference 2, the angle of incidence is 39° for a range of Mach numbers from 1.6 to ∞ . The calculations from the experimental data (h , R_p , t) indicated a rather large discrepancy (average angle of 58.1°). However, this angle was calculated by two different methods at two different heights of charge, h , and the results were fairly consistent. The geometric factor error does not enter into these determinations due to the small times and radii involved. Further investigation of this incidence angle was attempted at a charge height of three centimeters.

Clear photographs of the shock front system could not be obtained at this height due to the obliteration of the shock front by the explosive product gases at the radius of interest.

The magnitude of the geometric factor error described above was checked by calculating the corrected R_p using the formula;

$$R_p(\text{corrected}) = X \left(\sin \left(\tan^{-1} \left(\frac{R_p \cdot f}{Y} \right) \right) \right)$$

where X = distance from light to charge, Y = distance from light to grid screen, f = geometric factor and $R_p = R_p$ as given in table 1.

This calculation indicated the error was approximately 20% of the error shown for large R_p in Figures 18 and 19.

8. Bibliography

1. Tomlinson, W. R., Jr., as revised by Sheffield, O. E., Properties of Explosives of Military Interest, Picatinny Arsenal, Technical Report No. 1740, Revision 1, April 1958.
2. Kinney, G. F., Explosive Shocks in Air, New York; Macmillan Co., 1962.
3. Brode, H. L., A Calculation of the Blast Wave from a Spherical Charge of TNT, USAF Project Rand, RM-1965, 21 August 1957, (U-38125)
4. Glenn, D. W. and R. S. Salin, Mach Y-Stems form Spherical Shocks, Thesis G-459, U. S. Naval Postgraduate School, 1960.
5. Wilson, P. W., and C. J. Treat, Photographic Investigation of Air Shock Phenomena from Decigram Charges, Thesis w641, U. S. Naval Postgraduate School, 1959.
6. Edgerton, H. E., Shock Wave Photography of Large Subjects in Daylight, Review of Scientific Instruments, Feb. 1958, p171-172
7. Courant R. and K. O. Friedrichs, Supersonic Flow and Shock Fronts, Interscience Pub., 1948.
8. Stoner, R. G. and W. Bleakney, Attenuation of Spherical Shock Waves in Air, J. Appl. Phy., v19, 1948, p670-678.
9. Shardin, H., Measurements of Spherical Shock Waves, Commun. Pure and Appl. Math., New York Univ., vol. VII, 1954, p223-243.
10. Brode, H. L., Numerical Solutions of Spherical Blast Waves, J. Appl. Phy., v26, 1955, p776.

Delta ϵ vs Radius

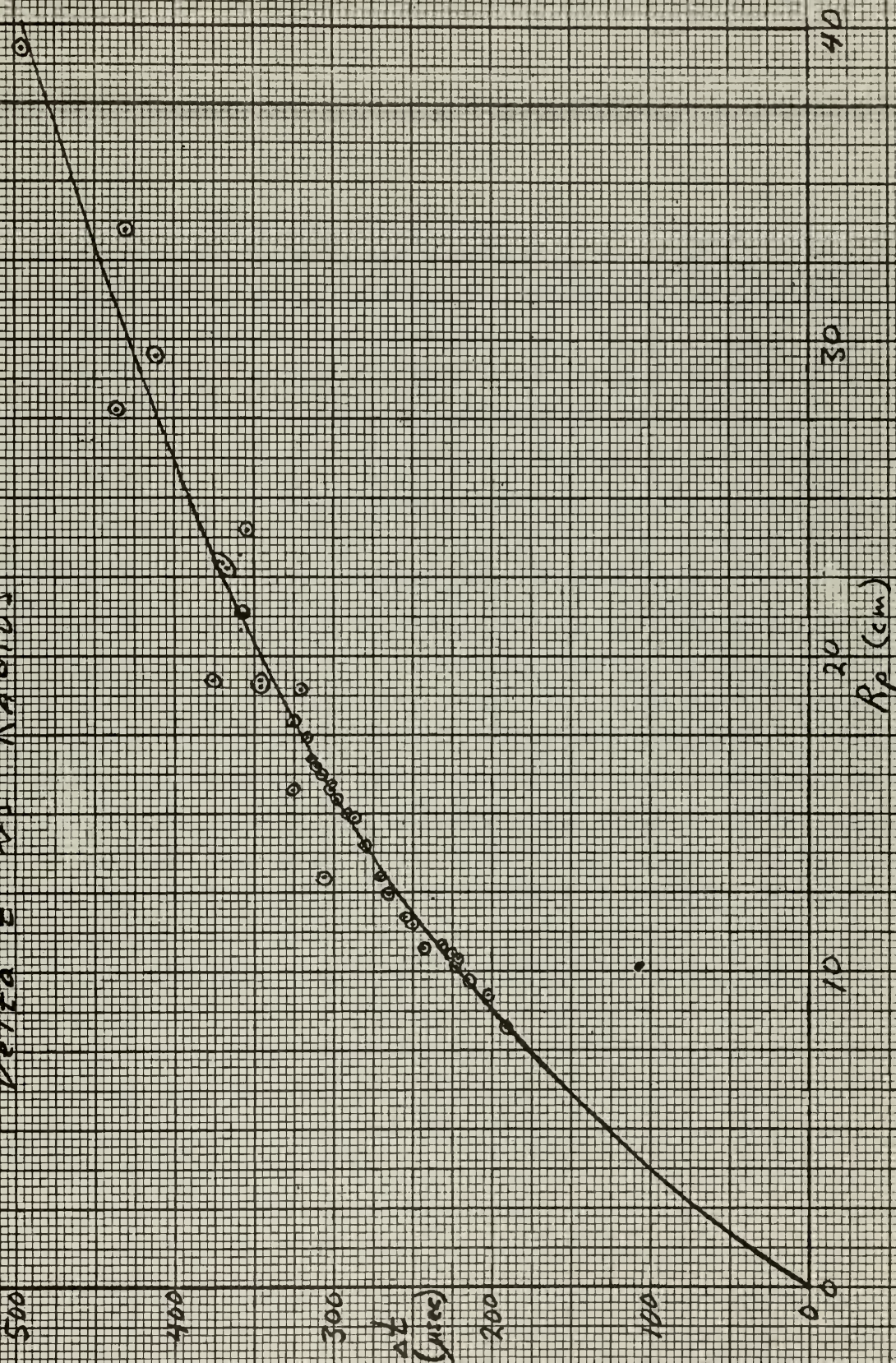


Figure 11

Height of Triple Point

vs Time

~~000~~ $h = 5 \text{ cm}$

~~000~~ $h = 8 \text{ cm}$

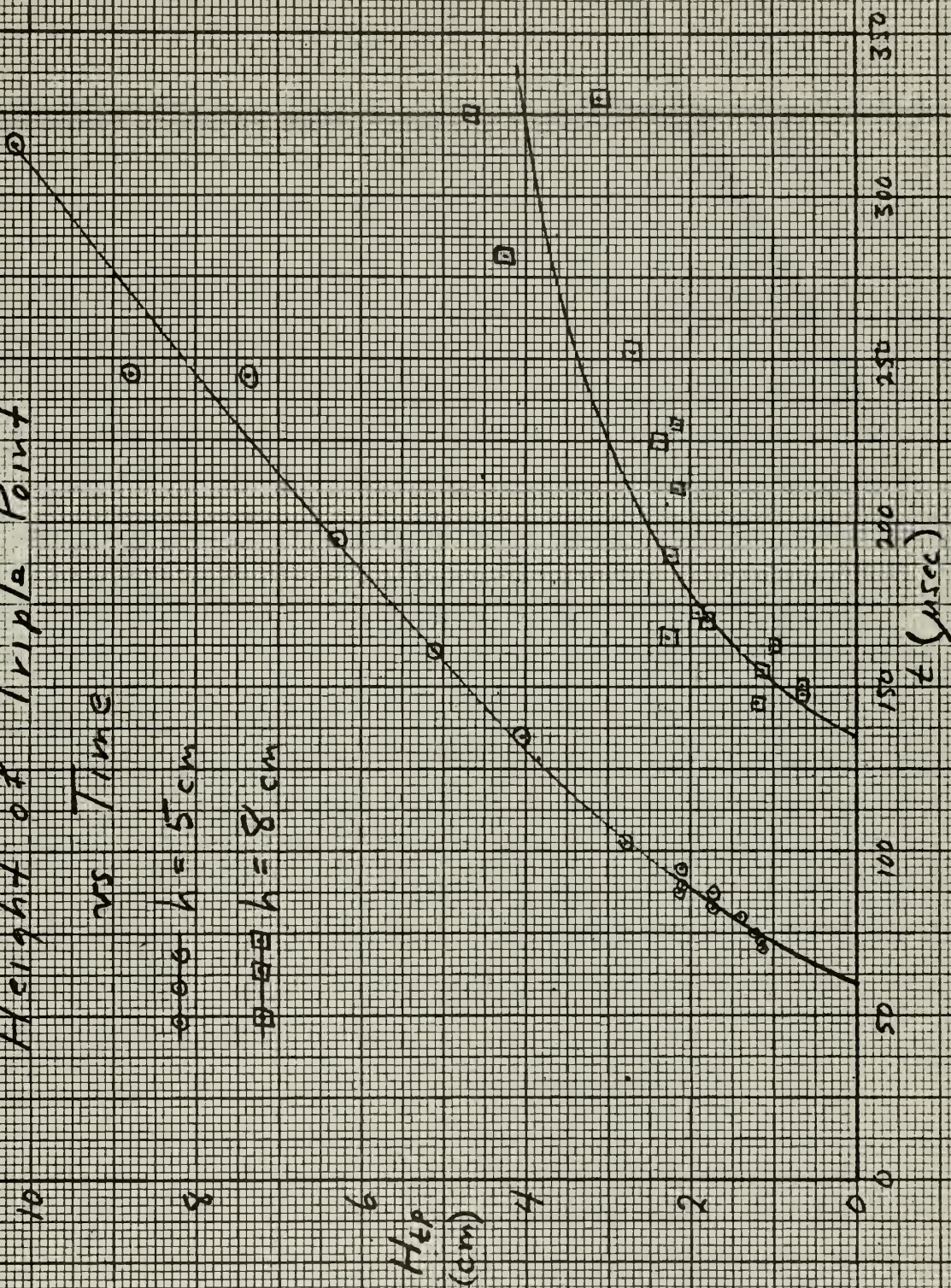


Figure 12

Distance of Mach Y-Stem from Ground Zero vs Time

5 cm

8 cm

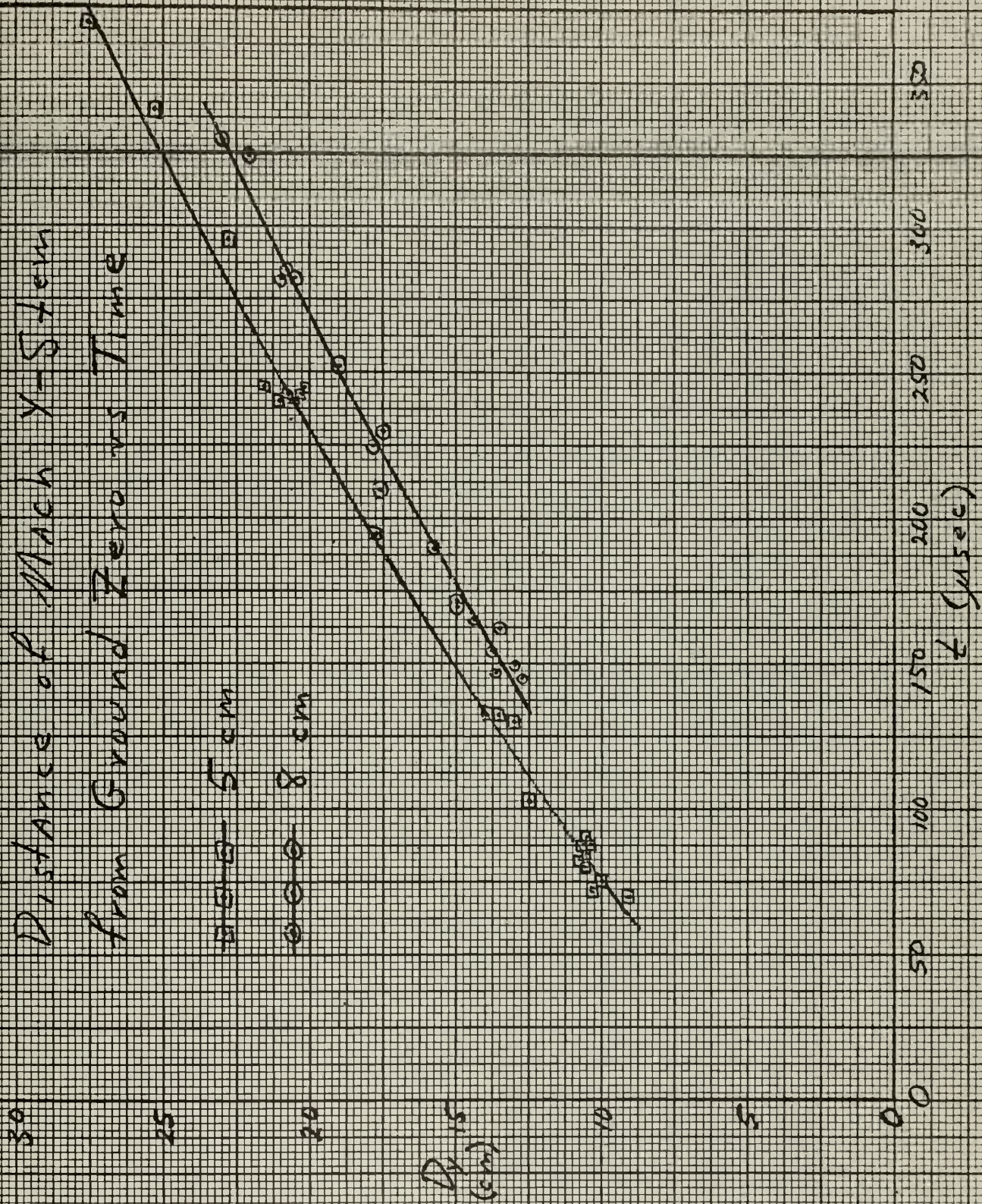


Figure 18

b Ratio vs Radius

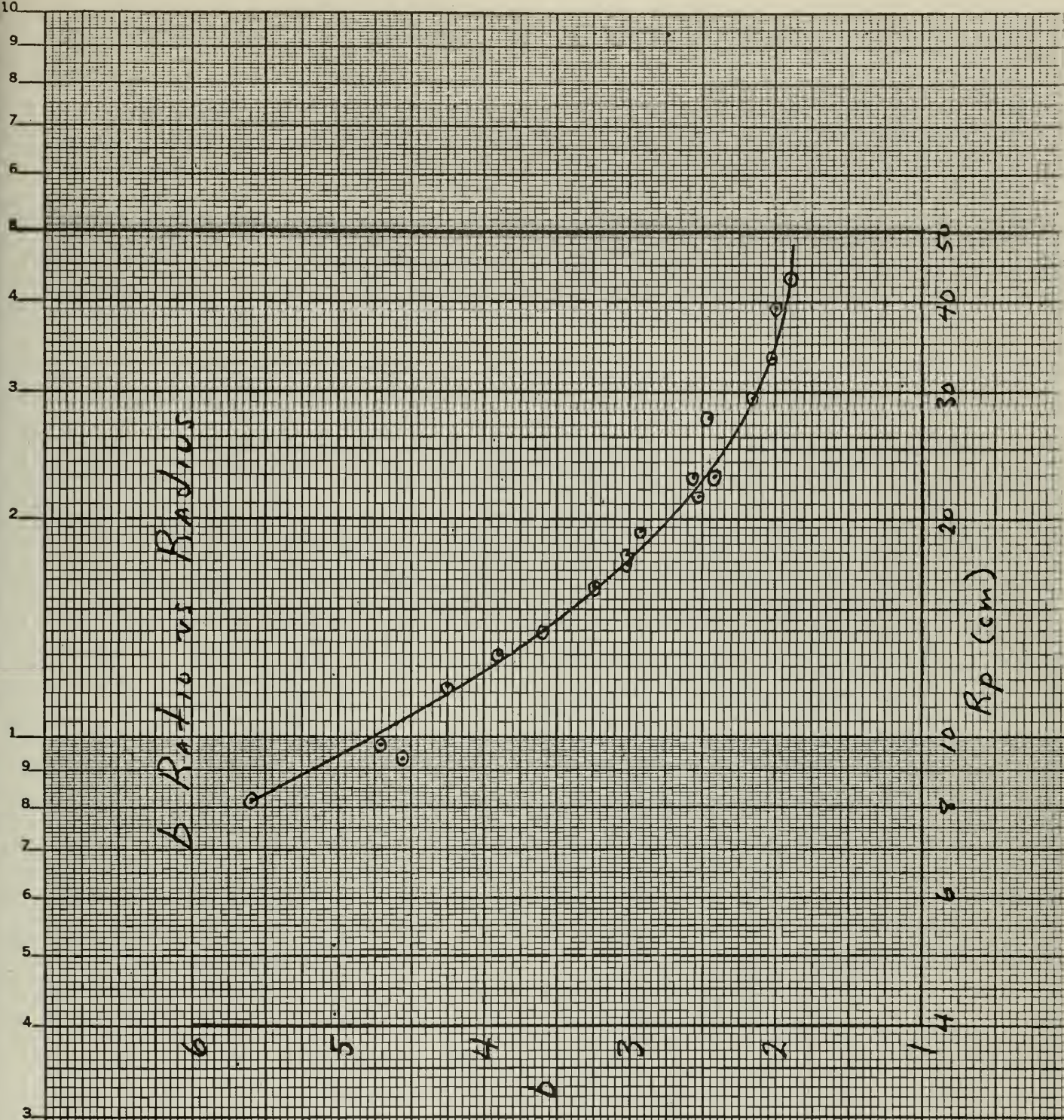


Figure 14

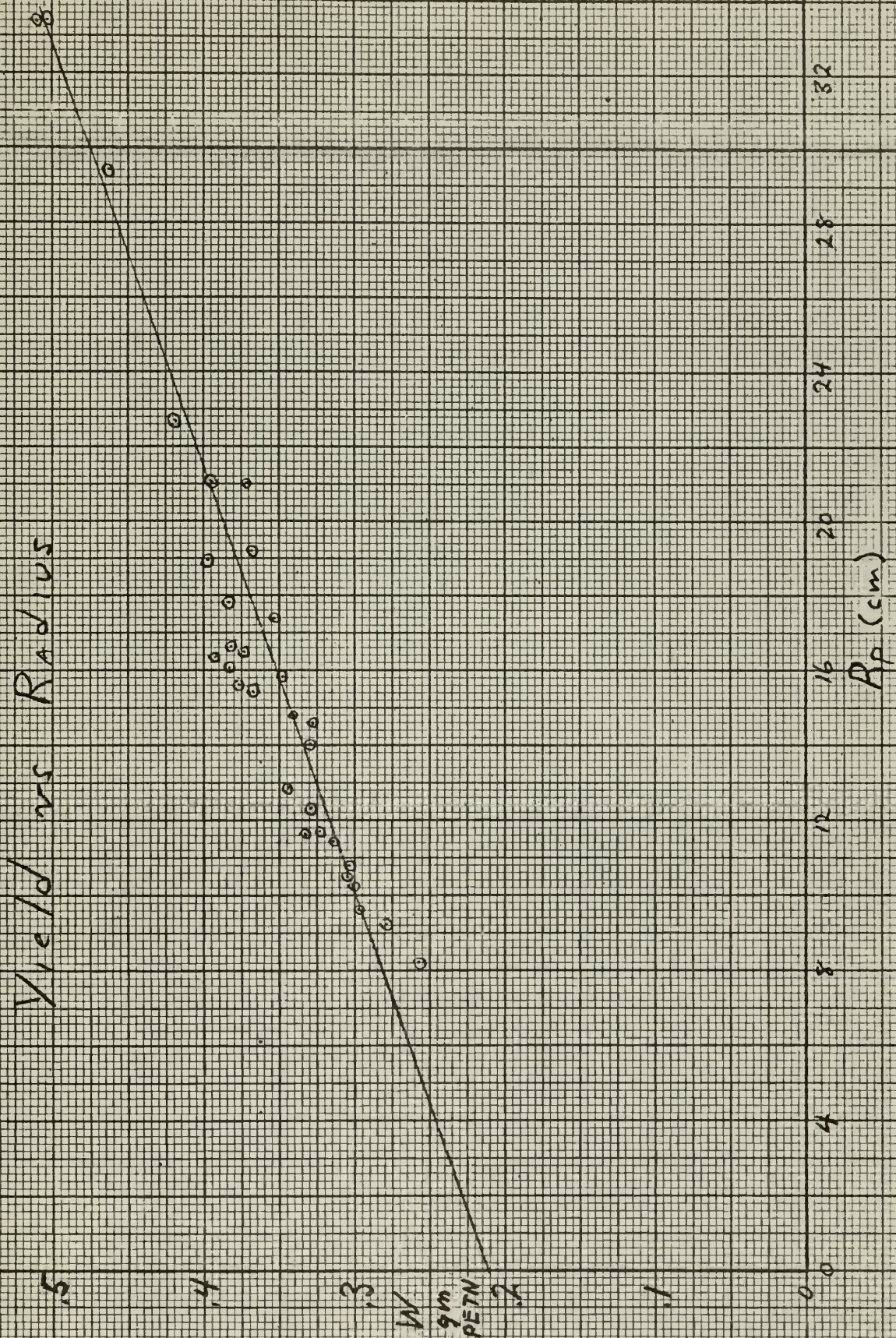


Figure 15

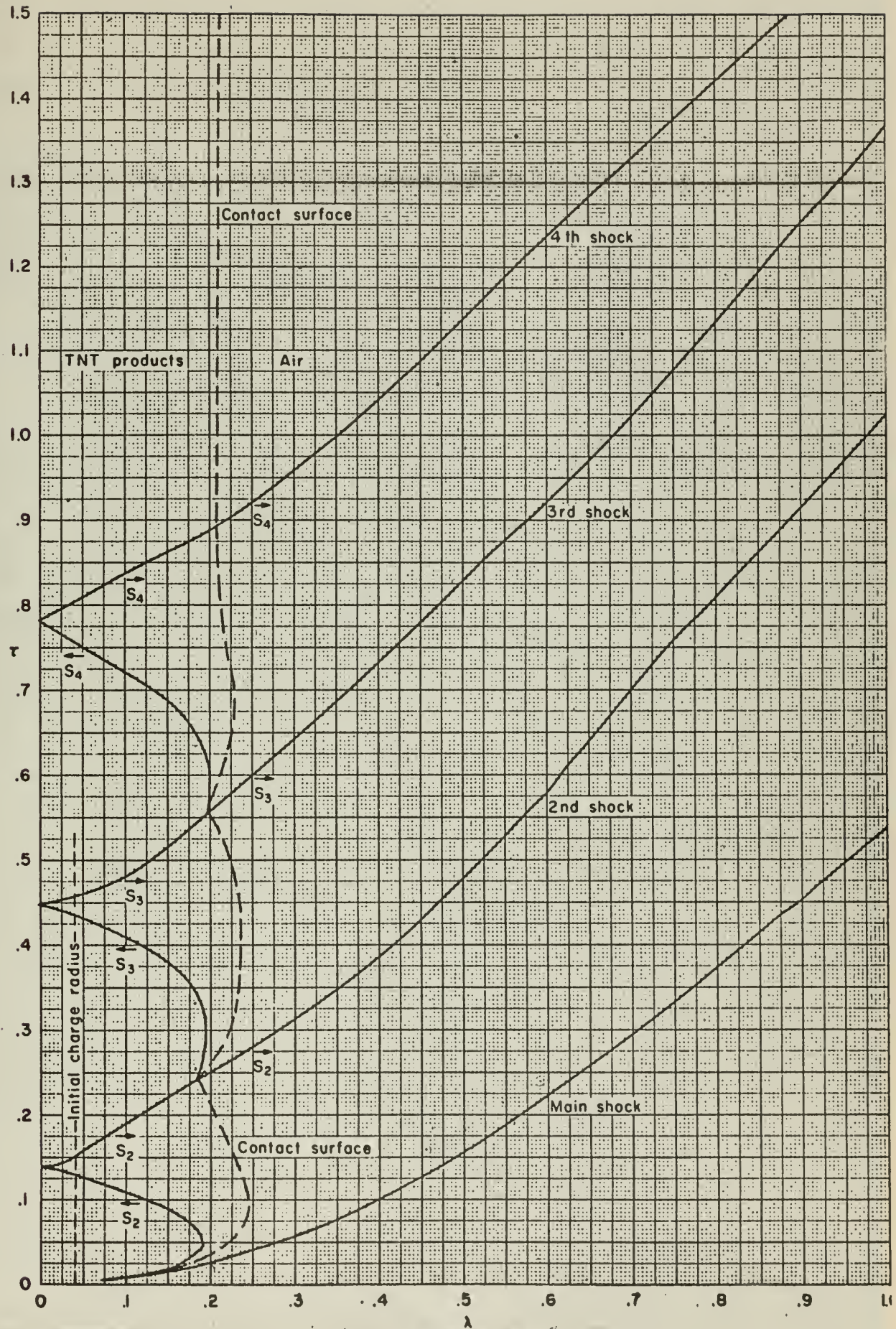


Figure 16

Overpressure vs Reduced Radius

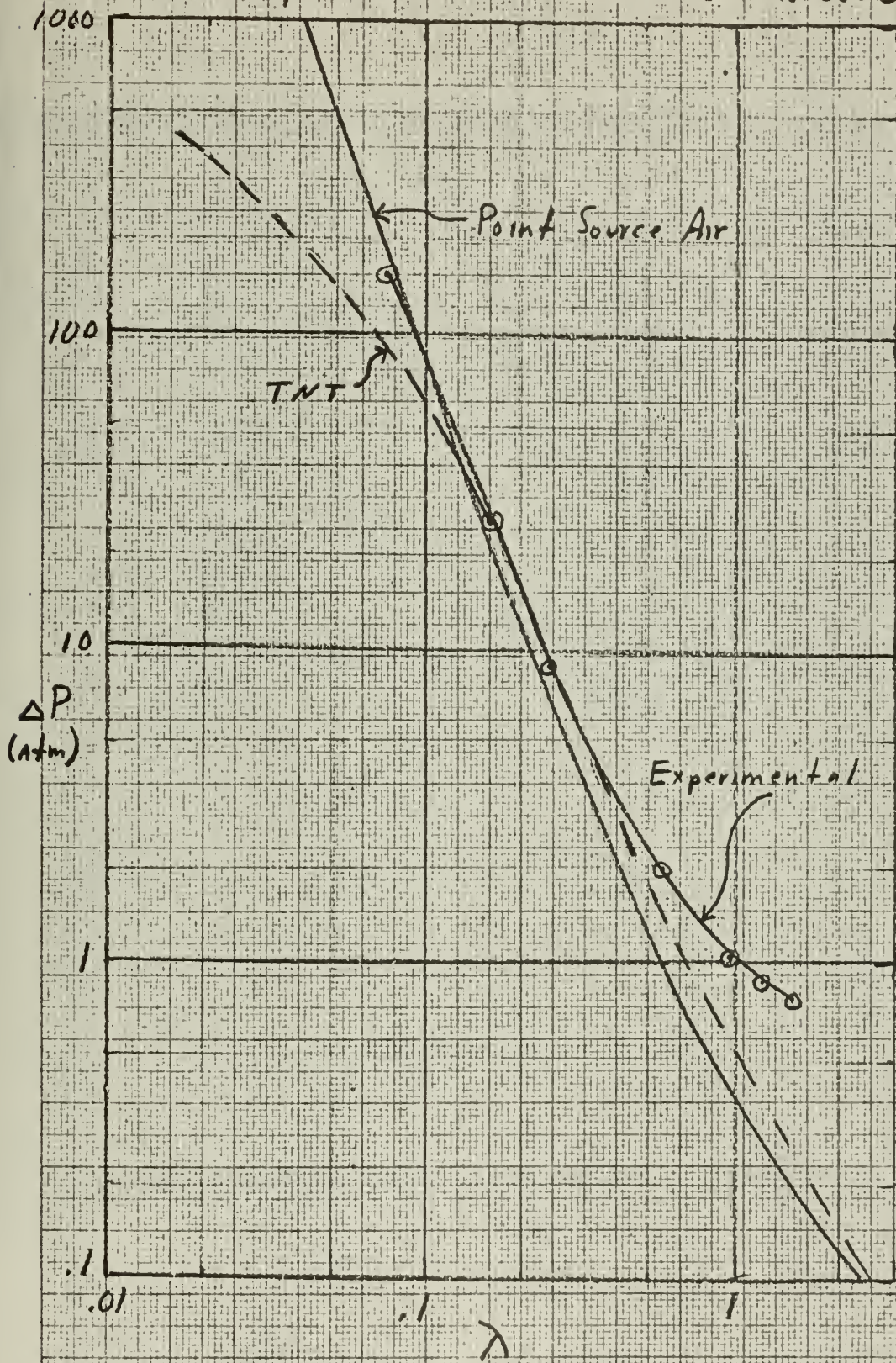


Figure 17

Reduced Time
vs
Reduced Radius

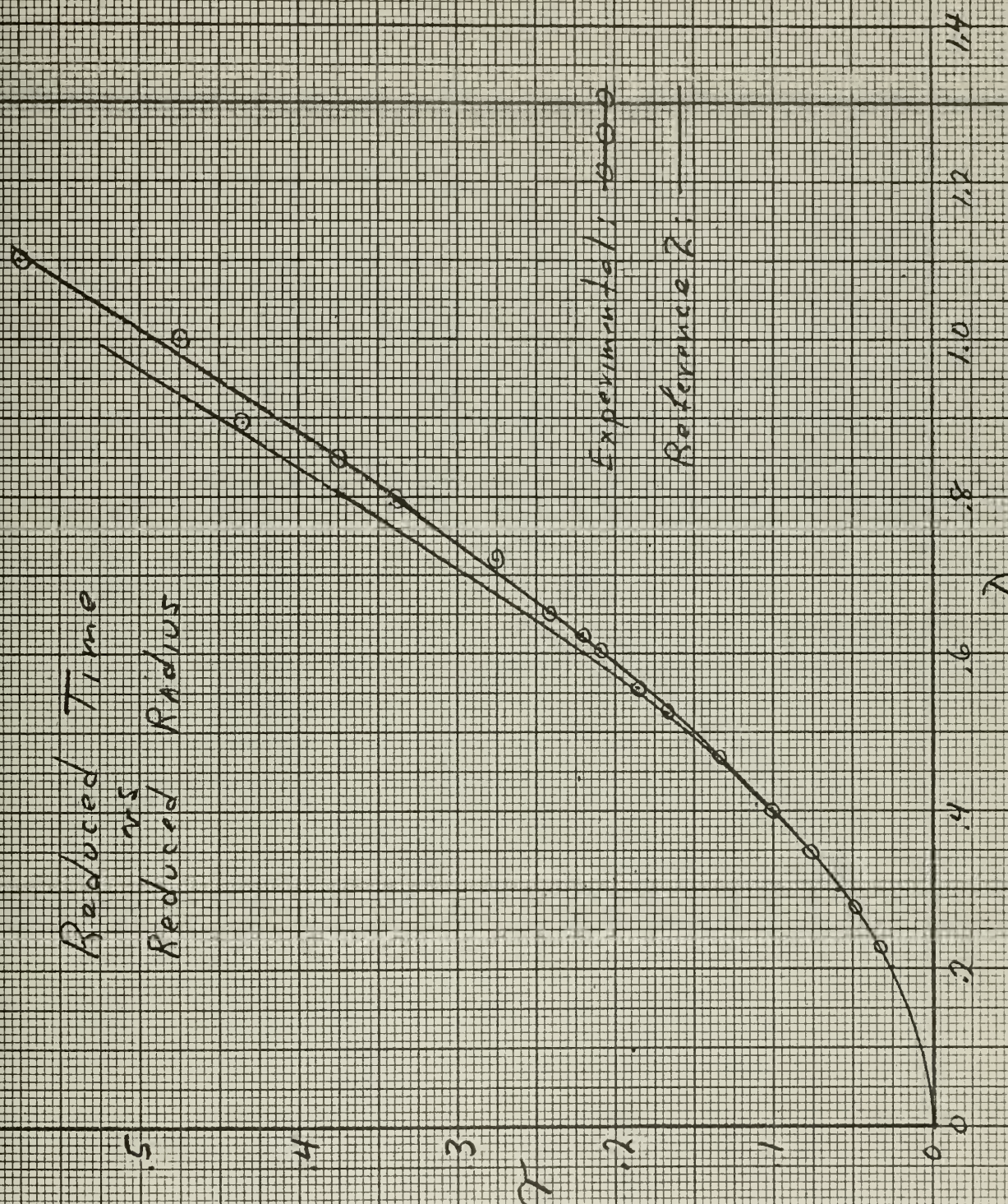
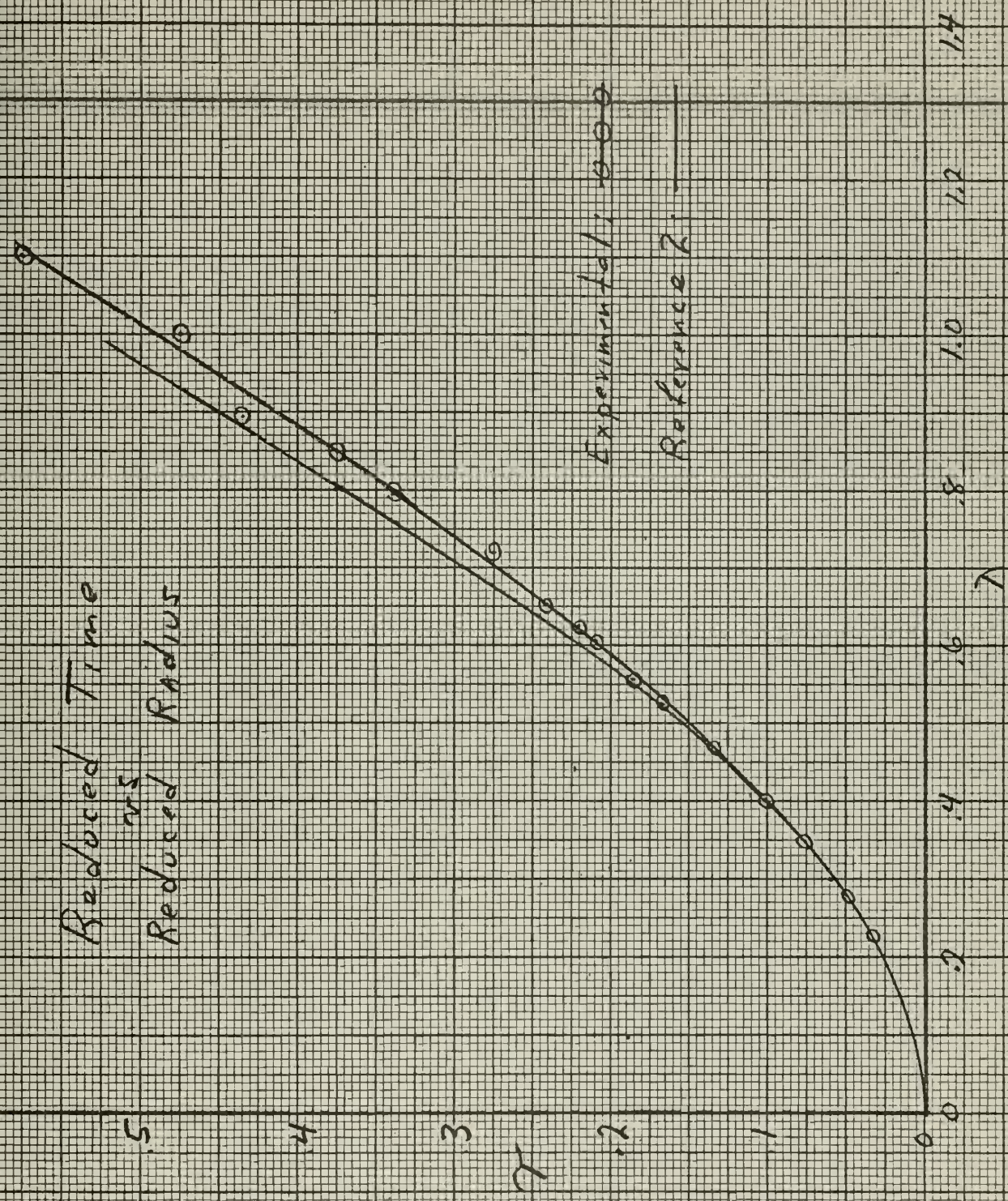


Figure 18

Reduced Time
vs
Reduced Radius



Experimental:

Reference 2:

Figure 18

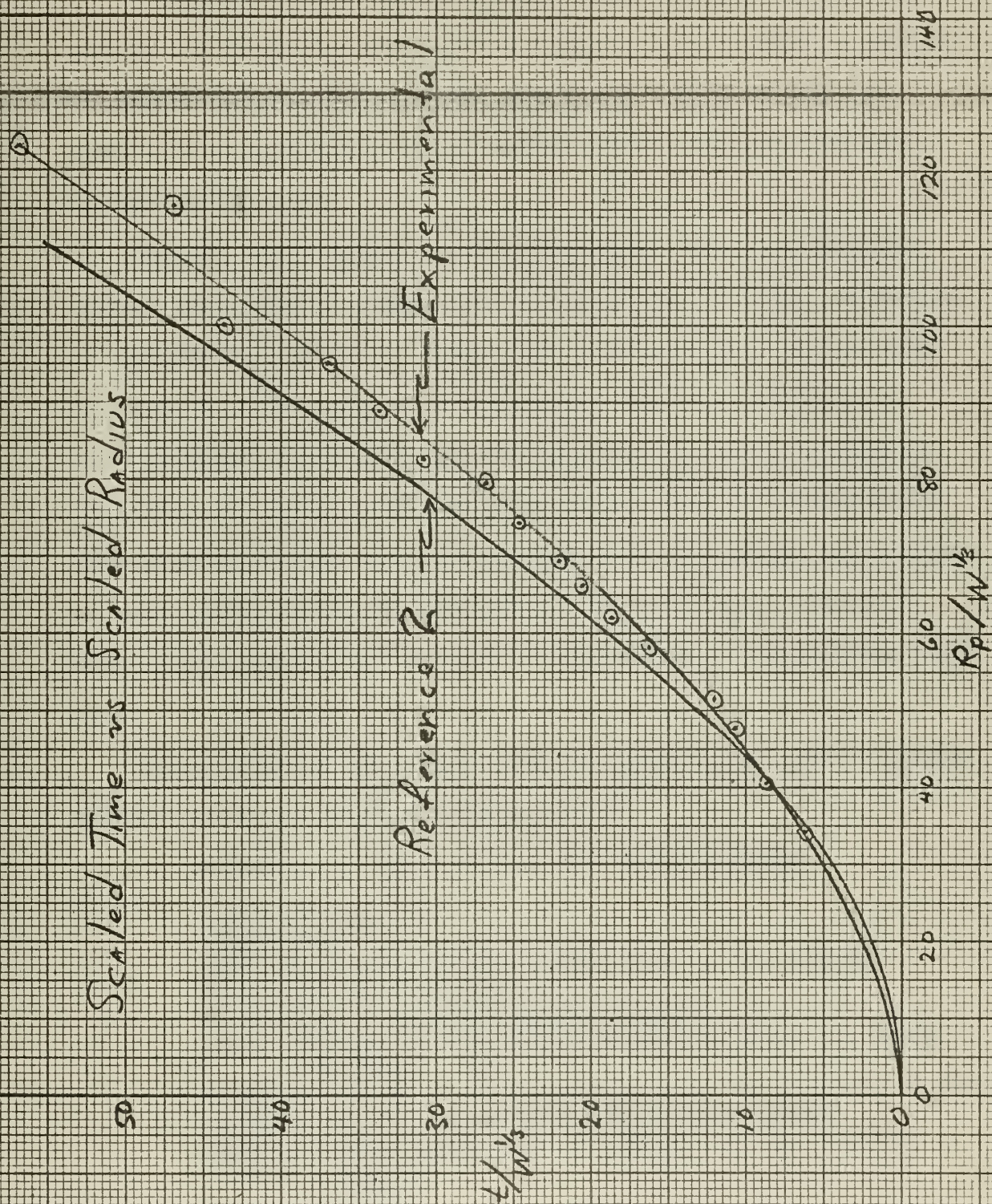


Figure 19

APPENDEK I

A Computer Data Corporation, Model 1604, Digital Computer was used to facilitate the numerous and repetitive calculations necessary to convert the raw data to useful parameters. The following discussion is an explanation of the method and the program utilized to accomplish the above.

Briefly, the programs, as described below, when used with the library taped BIMED 8 program, will take in the basic data, calculate all parameters used in the thesis, fit the best curves various order polynomials to the curve of Δt versus R_p , take the derivative of these polynomials and print out all input and calculated parameters. (See Table 2) Values of Δt for given values of R_p as calculated for each order polynomial were also printed out to facilitate the plotting of these curves. This was necessary to determine which polynomial most closely agreed with the plot of experimentally determined Δt and R_p .

That portion of the program that was added to the BIMED 8 program and the reason for doing so is given below.

A. Definition of the functions used in the program:

RPRIM(I) = R_p

TSET(I) = t

MM = total number of data points used in the program

PO = atmospheric pressure

WP = weight of PETN per charge in grams

WAZST = weight of lead azide and lead styphnate per charge
in grams

TJOULES = energy of explosion per charge in joules/gm of PETN

VSOUND = velocity of sound in standard atmosphere

WPTOTAL = total equivalents of PETN per charge in grams

SCALE = $(W/W_0)^{1/3}$

DELTA = ΔA

ALPHA = α

CONST1 = $7/8$

TARRIV(I) = t_a

RLAMB(I) = λ

$TRED(I) = \tau$
 $DELTT(I) = \Delta t$
 $BRATIO(I) = b$
 $DSCAL(I) = \text{scaled radius}$
 $TSCAL(I) = \text{scaled time}$
 $SLOPE(I) = d\Delta t/dR_p$
 $SMACH(I) = M$
 $APRES(I) = \Delta P \text{ in atmospheres}$

B. Description of program:

(1) The following was added directly to the front of the BIMED 8 program. This portion supplies R_p , t and various constants to the computer and calculates all parameters not dependent on the slope of the Δt versus R_p curve:

```

..JOB*LUSK   3 MIN MAX   BIGSHOCK
PROGRAM BIGSHOK
DIMENSION RLAMB(50), TARRV(50), DELTT(50), RPRIM(50),
1TRED(50), DSCAL(50), TSCAL(50), SMACH(50), APRES(50),
2SLOPE(50), BRATIO(50), Z(50)
MM = 36
READ 810, (RPRIM(I), TSET(I), I = 1,MM)
READ 701, (Z(I), I = 1,16)
PO = 14.6959
WP = .249
WAZST = .030
TJOULES = 7690.
VSOUND = .0343
WPTOTAL = WP + WAZST*.392/1.73
SCALE = (WPTOTAL*1.73/2000./453.6)**.33333
DELTA = TJOULES*WPTOTAL
ALPHA = DELTA*100./PO/.68946)**.33333
CONST1 = 7./6.
DO 820 I = 1,MM
TARRV(I) = RPRIM(I)/VSOUND
RLAMB(I) = RPRIM(I)/ALPHA
TRED(I) = TSET(I)*VSOUND/ALPHA
DELTT(I) = TARRV(I) - TSET(I)
BRATIO(I) = RPRIM(I)/TSET(I)/.001/2.54/12.
DSCAL(I) = RPRIM(I)/SCALE/2.54/12.
820 TSCAL(I) = TSET(I)/SCALE/1000.
810 FORMAT (E10.4, E20.4)
701 FORMAT (F5.1)

```

(2) The input statements of the BIMED 8 were modified thusly, to supply R_p and t as its input:

```

21 DO 19 I = 1,MM
X(I,1) = RPRIM(I)*100.0
19 X(I,NT) = DELTT(I)*100.0

```

(3) The following statements were added to the BIMED 8 immediately after it has determined all the coefficients of the polynomials. This portion of the program calculates the slope of the computer determined polynomials, the Mach number, the overpressure and then prints out all parameters for all values of R_p supplied as input. It also calculates and prints out the values of Δt for various R_p 's as calculated from each polynomial. This is done, as mentioned above, merely for ease of plotting these polynomials.

```

      PRINT 802
      DO 803 I = 1,16
      Y = A
      DO 804 J = 1,N1
804  Y = Y + B(J)*Z(I)**J
803  PRINT 805, Z(I), Y
      IF (N1-2) 70,826,826
826  IF (N1-4) 825,825,70
825  DO 850 I = 1,MM
      SLOPE(I) = B(1) + 2.0*B(2)*RPRIM(I) + 3.0*B(3)*RPRIM(I)**2
      + 4.0*B(4)*RPRIM(I)**3
      SMACH(I) = 1.0/(1.0-VSOUND*SLOPE(I))
850  APRES(I) = (SMACH(I)**2 - 1.0)*CONST1
      PRINT 870, WPTOTAL, DELTA, ALPHA, SCALE
      PRINT 871, N1
      PRINT 872, B(1), B(2), B(3), B(4)
      PRINT 860
      PRINT 865, (RPRIM(I), TSET(I), TARRV(I), DELTT(I), RLAMB(I),
1TRED(I), DSCAL(I), TSCAL(I), SLOPE(I), SMACH(I), APRES(I),
2BRATIO(I), I = 1,MM)
      PRINT 866
802  FORMAT (1H0 5HRPRIM 5X 5HDELTT/)
805  FORMAT (2F10.3)
870  FORMAT (9H1WPTOTAL= F8.6, 11H      DELTA= F9.3, 11H      ALPHA=
1F10.6, 11H      SCALE= F7.5///)
871  FORMAT (90DATA FOR I2, 18H DEGREE POLYNOMIAL/)
872  FORMAT (9HOSLOPE= F9.5, 7H + 2.0( F9.5, 13H)RPRIM + 3.0(
1F9.5, 16H)RPRIM**2 + 4.0( F9.5, 9H)RPRIM**3///)
860  FORMAT (12OH0      RPRIM      TSET      TARRV      DELTT
2RLAMB      TRED      DSCAL      TSCAL      SLOPE      SMACH
3APRES      BRATIO)
866  FORMAT (1H1)

```

WPTOTAL= .255850

DELTA= 1967.484

ALPHA= 26.789993

SCALE= .00787

DATA FOR 4 DEGREE POLYNOMIAL

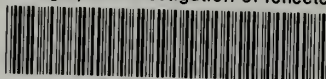
SLOPE = $30.20447 + 2.0(-.95667)RPRIM + 3.0(.01889)RPRIM^2 +$
 $4.0(-.00015)RPRIM^3$

| RPRIM | TSET | TARRV | DELTT | RLAMB | TRED | DSCAL |
|--------|---------|---------|---------|-------|------|--------|
| .000 | .000 | .000 | .000 | .000 | .000 | .000 |
| 8.220 | 48.300 | 239.650 | 191.350 | .307 | .062 | 34.255 |
| 9.280 | 67.000 | 270.554 | 203.554 | .346 | .086 | 38.673 |
| 9.750 | 68.000 | 284.257 | 216.257 | .364 | .087 | 40.631 |
| 10.370 | 80.300 | 302.332 | 222.032 | .387 | .103 | 43.215 |
| 10.510 | 80.900 | 306.414 | 225.514 | .392 | .104 | 43.798 |
| 10.820 | 83.400 | 315.452 | 232.052 | .404 | .107 | 45.090 |
| 11.470 | 84.900 | 334.402 | 249.502 | .428 | .109 | 47.799 |
| 11.690 | 88.000 | 340.816 | 252.816 | .436 | .113 | 48.716 |
| 11.780 | 90.900 | 343.440 | 252.540 | .440 | .116 | 49.091 |
| 12.400 | 95.000 | 361.516 | 266.516 | .463 | .122 | 51.675 |
| 13.000 | 110.000 | 379.009 | 269.009 | .485 | .141 | 54.175 |
| 13.100 | 110.000 | 381.924 | 271.924 | .489 | .141 | 54.592 |
| 14.000 | 128.000 | 408.163 | 280.163 | .523 | .164 | 58.342 |
| 14.100 | 131.400 | 411.079 | 279.679 | .526 | .168 | 58.759 |
| 14.800 | 144.100 | 431.487 | 287.387 | .552 | .184 | 61.676 |
| 14.870 | 147.100 | 433.528 | 286.428 | .555 | .188 | 61.968 |
| 15.450 | 151.500 | 450.437 | 298.937 | .577 | .194 | 64.385 |
| 15.730 | 156.000 | 458.601 | 302.601 | .587 | .200 | 65.552 |
| 15.900 | 162.000 | 463.557 | 301.557 | .594 | .207 | 66.260 |
| 16.220 | 164.000 | 472.886 | 308.886 | .605 | .210 | 67.594 |
| 16.400 | 165.700 | 478.134 | 312.434 | .612 | .212 | 68.344 |
| 16.560 | 171.000 | 482.799 | 311.799 | .618 | .219 | 69.010 |
| 16.720 | 173.300 | 487.464 | 314.164 | .624 | .222 | 69.677 |
| 17.430 | 190.000 | 508.163 | 318.163 | .651 | .243 | 72.636 |
| 17.850 | 194.200 | 520.408 | 326.208 | .666 | .249 | 74.386 |
| 19.112 | 211.000 | 557.201 | 346.201 | .713 | .270 | 79.645 |
| 19.250 | 215.000 | 561.224 | 346.224 | .719 | .275 | 80.221 |
| 19.310 | 225.000 | 562.974 | 337.974 | .721 | .288 | 80.471 |
| 19.840 | 242.800 | 578.426 | 335.626 | .741 | .311 | 82.679 |
| 21.300 | 265.000 | 620.991 | 355.991 | .795 | .339 | 88.763 |
| 22.750 | 295.900 | 663.265 | 367.365 | .849 | .379 | 94.806 |
| 22.780 | 293.900 | 664.140 | 370.240 | .850 | .376 | 94.931 |

| RPRIM | TSET | TSCAL | SLOPE | SMACH | APRES | BRATIO |
|--------|---------|--------|--------|---------|-----------|--------|
| .000 | .000 | .000 | 30.204 | -27.768 | 13202.415 | .000 |
| 8.220 | 48.300 | 6.135 | 17.569 | 2.606 | 99.323 | 5.584 |
| 9.280 | 67.000 | 8.510 | 16.844 | 2.368 | 79.010 | 4.544 |
| 9.750 | 68.000 | 8.637 | 16.374 | 2.281 | 72.069 | 4.704 |
| 10.370 | 80.300 | 10.200 | 15.780 | 2.180 | 64.324 | 4.237 |
| 10.510 | 80.900 | 10.276 | 15.650 | 2.159 | 62.763 | 4.262 |
| 10.820 | 83.400 | 10.593 | 15.367 | 2.115 | 59.520 | 4.256 |
| 11.470 | 84.900 | 10.784 | 14.798 | 2.031 | 53.557 | 4.432 |
| 11.690 | 88.000 | 11.178 | 14.612 | 2.005 | 51.760 | 4.358 |
| 11.780 | 90.900 | 11.546 | 14.537 | 1.994 | 51.054 | 4.252 |
| 12.400 | 95.000 | 12.067 | 14.035 | 1.928 | 46.602 | 4.282 |
| 13.000 | 110.000 | 13.572 | 13.574 | 1.871 | 42.888 | 3.877 |
| 13.100 | 110.000 | 13.972 | 13.500 | 1.862 | 42.319 | 3.907 |
| 14.000 | 128.000 | 16.258 | 12.859 | 1.789 | 37.733 | 3.588 |
| 14.100 | 131.400 | 16.690 | 12.791 | 1.782 | 37.278 | 3.521 |
| 14.800 | 144.100 | 18.303 | 12.331 | 1.733 | 34.347 | 3.370 |
| 14.870 | 147.100 | 18.685 | 12.287 | 1.728 | 34.077 | 3.317 |
| 15.450 | 151.500 | 19.243 | 11.931 | 1.693 | 31.981 | 3.346 |
| 15.730 | 156.000 | 19.815 | 11.766 | 1.677 | 31.054 | 3.308 |
| 15.900 | 162.000 | 20.577 | 11.668 | 1.667 | 30.515 | 3.220 |
| 16.220 | 164.000 | 20.831 | 11.488 | 1.650 | 29.548 | 3.245 |
| 16.400 | 165.700 | 21.047 | 11.389 | 1.641 | 29.030 | 3.247 |
| 16.560 | 171.000 | 21.720 | 11.303 | 1.633 | 28.584 | 3.177 |
| 16.720 | 173.300 | 22.012 | 11.218 | 1.625 | 28.151 | 3.165 |
| 17.430 | 190.000 | 24.134 | 10.856 | 1.593 | 26.379 | 3.010 |
| 17.850 | 194.200 | 24.667 | 10.654 | 1.576 | 25.434 | 3.016 |
| 19.112 | 211.000 | 26.801 | 10.098 | 1.530 | 22.983 | 2.972 |
| 19.250 | 215.000 | 27.309 | 10.041 | 1.525 | 22.746 | 2.937 |
| 19.310 | 225.000 | 28.579 | 10.017 | 1.523 | 22.645 | 2.816 |
| 19.840 | 242.800 | 30.840 | 9.809 | 1.507 | 21.793 | 2.681 |
| 21.300 | 265.000 | 33.660 | 9.293 | 1.468 | 19.799 | 2.637 |
| 22.750 | 295.900 | 37.585 | 8.857 | 1.436 | 18.228 | 2.522 |
| 22.780 | 293.900 | 37.331 | 8.849 | 1.436 | 18.199 | 2.543 |

thesL915

Photographic investigation of reflected



3 2768 002 12416 6

DUDLEY KNOX LIBRARY